Mon. Not. R. Astron. Soc. **376,** 1588–1610 (2007) doi:10.1111/j.1365-2966.2007.11570.x

Molecular cloud regulated star formation in galaxies

C. M. Booth,[1⋆] Tom Theuns[1,2] and Takashi Okamoto[1,3]

[1] *Institute for Computational Cosmology, University of Durham, South Road, Durham DH1 3LE*
[2] *University of Antwerp, Campus Groenenborger, Groenenborgerlaan 171, B-2020 Antwerpen, Belgium*
[3] *Division of Theoretical Astronomy, National Astronomical Observatory of Japan, 2-21-1 Osawa, Mitaka, Tokyo 181-8588, Japan*

Accepted 2007 January 30. Received 2007 January 24; in original form 2006 October 20

ABSTRACT

We describe a numerical implementation of star formation in disc galaxies, in which the conversion of cooling gas to stars in the multiphase interstellar medium is governed by the rate at which molecular clouds are formed and destroyed. In the model, clouds form from thermally unstable ambient gas and get destroyed by feedback from massive stars and thermal conduction. Feedback in the ambient phase cycles gas into a hot galactic fountain or wind. We model the ambient gas hydrodynamically using smoothed particle hydrodynamics. However, we cannot resolve the Jeans mass in the cold and dense molecular gas and, therefore, represent the cloud phase with ballistic particles that coagulate when colliding. We show that this naturally produces a multiphase medium with cold clouds, a warm disc, hot supernova bubbles and a hot, tenuous halo. Our implementation of this model is based on the GADGET *N*-body code. We illustrate the model by evolving an isolated Milky Way-like galaxy and study the properties of a disc formed in a rotating spherical collapse. Many observed properties of disc galaxies are reproduced well, including the molecular cloud mass spectrum, the molecular fraction as a function of radius, the Schmidt law, the stellar density profile and the appearance of a galactic fountain.

Key words: methods: *N*-body simulations – galaxies: formation – galaxies: ISM.

1 INTRODUCTION

Galaxies form when gas cools radiatively inside a dark matter (DM) halo. The haloes in turn form from the non-linear collapse of initially small density perturbations that were imprinted by quantum fluctuations before inflation. When the virial temperature of the halo is high enough, the gas can cool radiatively (Rees & Ostriker 1977; White & Rees 1978) and may become self-gravitating. Some fraction of the cooling gas can form stars, which then affect the baryon distribution and star formation rate (SFR) through feedback, for example, from supernova (SN) explosions (e.g. Dekel & Silk 1986).

Simulating the growth of DM haloes from initially small cosmological density perturbations has become routine to the extent that even the complex non-linear stage can be predicted with relative confidence (e.g. Springel et al. 2005). However, following the behaviour of the baryons until stars form is much more demanding for two main reasons. First, the physical processes that lead to star formation are still relatively poorly understood, even in the Milky Way (MW). Stars are thought to form in molecular clouds in a complex interstellar medium (ISM) in which magnetic fields (Safier, McKee & Stahler 1997), cosmic rays, turbulence (Krumholz & McKee 2005), relativistic jets (Klamer et al. 2004), molecules, dust, and radiative transfer may all play some role. Secondly, the physical scales on which star formation takes place is vastly different from those of cosmological interest. Therefore, simulations on a sufficiently large scale to sample cosmological structures cannot presently also resolve physics on the scales relevant for star formation. For these two reasons, simulations invariably include 'sub-grid' physics that model the complexity of star formation in the ISM using simple rules.

In the first generation of hydrodynamic models for galaxy formation (Cen & Ostriker 1992; Navarro & White 1993; Steinmetz & Muller 1994; Katz, Weinberg & Hernquist 1996), the gaseous component of galaxies is modelled as a single fluid. Because the spatial and mass resolution in these simulations is insufficient to resolve star formation they rely on a simple star formation prescription. In its simplest form, this consists of devising criteria by which simulated gas can be flagged as eligible to form stars and then converting the gas to stars by hand (see e.g. Kay et al. 2002, for a comparison of such criteria). Feedback from core collapse (type II) SNe, modelled as an extra source of thermal or kinetic energy, was found to have little effect in the early models. This is because the gas in the surroundings of star formation sites is at high density and so is very efficient at just radiating away the added energy. As a consequence, too much gas cooled in dense knots, producing galaxies much more

⋆E-mail: c.m.booth@durham.ac.uk

© 2007 The Authors. Journal compilation © 2007 RAS

concentrated than those observed (Navarro & Benz 1991; Weil, Eke & Efstathiou 1998).

The ISM in observed galaxies is much more complex than the single-phase medium present in these early simulations. Although observed galaxies may have comparable mean gas density to the simulated ones, the real ISM consists of very dense cold clouds with small volume filling factor, embedded in a much more tenuous low-density, hot medium with a 'warm' phase at the interface. SN explosions in the tenuous medium have a much greater impact on the galaxy because this medium cools much less efficiently than gas at the mean density. Throughout this work, we will use the label 'cold' to describe the molecular clouds in the ISM, and the labels 'warm' and 'hot' to describe the properties of the ambient gas phase at temperatures of approximately 10^4 and 10^6 K, respectively.

In response to these problems with the simplest star formation and feedback criteria several authors have introduced 'multiphase' models for star formation in which the ISM is treated as a number of distinct phases. These schemes take various forms including modification of the simulation algorithm (Croft et al. 2000; Ritchie & Thomas 2001; Scannapieco et al. 2006), treating the multiphase medium implicitly by formulating differential equations that model the interactions between the phases (Yepes et al. 1997; Springel & Hernquist 2003; Okamoto et al. 2005), explicitly decoupling SN-heated gas from its surroundings (Stinson et al. 2006) or by decoupling the cold molecular phase from the hot phase by one of a variety of methods, including 'sticky particles' (Semelin & Combes 2002; Harfst, Theis & Hensler 2006) or removing 'cold' particles from the smoothed particle hydrodynamics (SPH) calculation (Hultman & Pharasyn 1999; Pearce et al. 1999, 2001; Marri & White 2003). The decoupling of the hot and cold ISM phases allows thermal heating from SN feedback to become more efficient (due to the much lower density of the hot phase) and also allows one to follow the properties of the cold molecular phase of the ISM.

This paper describes an attempt to mimic the multiphase medium in a star-forming galaxy. Since stars are known to form in molecular clouds, our method focuses on simple rules for cloud formation. The star formation recipe then simply converts the most massive of these clouds, 'Giant Molecular Clouds' (GMCs), into stars with an imposed efficiency taken from MW observations. Once a GMC forms stars stellar feedback destroys the cloud. We do not attempt to model the clouds themselves using hydrodynamics, because our current galaxy formation simulations lack by some margin the dynamic range to resolve the Jeans mass ($M_{\rm J}$) in the cold, dense gas that makes up the clouds. We can demonstrate this lack of resolution by considering theoretical models of the ISM (e.g. Wolfire et al. 1995), who calculated the thermal equilibrium gas properties of a diffuse ISM. Wolfire et al. (1995) found that a stable two-phase medium was produced, with a transition from hot material at densities $<10^{-0.5}$ cm^{-3} to cold, molecular material at densities $>10^{1.5}$ cm^{-3}. The Jeans mass of the warm ($T = 10^4$ K) phase is approximately 1×10^8 M$_\odot$, whereas the Jeans mass of the cold molecular gas ($T = 100$ K) is ~ 2000 M$_\odot$. Typical cosmological galaxy simulations currently have mass resolutions no better than 10^6 M$_\odot$ (Okamoto et al. 2005), many orders of magnitude away from being able to resolve the relevant scales for accurate tracking of the cold molecular phase. Note that these simulations do, however, resolve $M_{\rm J}$ in the warm phase. Given this limitation, we are forced to instead introduce another particle type in our simulations, called a 'sticky particle', to represent the clouds. These move as ballistic particles through the ambient medium, yet when they encounter another sticky particle interact inelastically based on a set of collision rules that mimic the coagulation of clouds. Sticky particles have been used before for similar reasons by, for example, Lin & Pringle (1976), Jenkins & Binney (1994) and Semelin & Combes (2002), and seem to have been introduced originally by Larson (1978) and Levinson & Roberts (1981). We show below that our imposed collision rules produce cloud statistics that are similar to those determined in nearby galaxies, for which they can be measured.

We begin by giving a brief overview of the current theory of the ISM and the formation of clouds, on which our recipes are based (Section 2). We then introduce the physics we model with the sticky particle prescription (Section 3), and constrain all of the free parameters in the model (Section 4). We then present results from simple isolated galaxy simulations (Section 5) and investigate the effects of changing the physics in the sticky particle model (Section 5.3). Section 6 contains conclusions and details of future work. The ISM is a complicated system and the nomenclature used to describe it is correspondingly complex. For this reason Appendix A contains a list of symbols and their associated meanings. Readers not interested in numerical details can read the summary of the model in Section 3 and then directly proceed to the analysis of the properties of the simulated galaxies presented in Section 5.

2 STAR FORMATION IN DISC GALAXIES

2.1 The interstellar medium in disc galaxies

According to the models of McKee & Ostriker (1977) (hereafter MO77; see also Efstathiou 2000; Monaco 2004; Krumholz & McKee 2005), the ISM of the MW consists of at least three separate and distinct gas phases: a hot tenuous medium at a temperature of $\sim 10^6$ K, cold, dense molecular clouds at a temperature of $\leqslant 100$ K and a warm medium that exists at the boundaries between clouds and the hot medium with $T \sim 10^4$ K. In the MW, the hot medium has a filling factor of 70–80 per cent and the cold clouds account for a few per cent of the volume (MO77). Different techniques are used to observe these different phases, with radio observations probing roto-vibrational transitions of molecules (mainly CO), the 21-cm line probing atomic hydrogen, and ultraviolet (UV) and X-ray observations probing the hot phase (see e.g. Binney & Merrifield 1998 for an overview and further references). The fact that different techniques are used to observe the different gas phases might exaggerate the degree to which these phases are really distinct.

Observations of star formation in the MW show that most stars form in groups, either as gravitationally bound clusters or as unbound associations, in the most massive of the molecular clouds (GMCs), with masses $\sim 10^6$ M$_\odot$, and sizes of the order of 30–50 pc (see e.g. Blitz & Thaddeus 1980 and Lada & Lada 2003 for recent reviews). The relatively small sizes of GMCs currently limit detailed observations of such clouds to nearby galaxies, with recent surveys done in the MW (Solomon et al. 1987; Heyer, Carpenter & Snell 2001), M33 (Rosolowsky & Blitz 2004) and the Large Magellanic Cloud (Fukui et al. 2001).

Blitz et al. (2006) present detailed observations of GMCs in five local galaxies. GMCs are excellent tracers of spiral structure to the extent that they are often used to *define* the location of arms, in a similar way as, for example, H II regions or massive stars are. There is a good correlation between the locations of GMCs and filaments of H I, although H I is often observed without accompanying molecular clouds, suggesting that the clouds form from H I.

Observations in more distant galaxies are currently limited to measuring the mean surface density of molecular gas with more

detailed observations awaiting new instruments such as ALMA.[1] According to Young & Scoville (1991), the fraction of gas in the molecular phase depends on Hubble type, with early-type spirals tending to be predominantly molecular and late types atomic. Optically barred spirals show a clear enhancement of CO emission along the bar. This suggests that the large-scale structure of the galaxy affects the formation of clouds and hence, presumably, also the SFR. A physical implementation of star formation should therefore aim to track the formation and evolution of molecular clouds. But how do GMCs form?

2.2 The formation of molecular clouds

Although the early models by Field, Goldsmith & Habing (1969) assumed that the different phases of the ISM were in pressure equilibrium, modern observations paint a picture of a much more complex and dynamic situation in which the ISM is shaped by turbulence, possibly powered by SNe and the large-scale dynamics of the galactic disc itself (see e.g. Burkert 2006 for a recent review). A galaxy-wide effect seems to be required to explain the observed Hubble-type dependence of cloud properties.

Yet how GMCs form in this complex environment is not well understood (Blitz & Rosolowsky 2004). Some authors have suggested that GMCs form by the coagulation of preexisting molecular clouds (Oort 1954; Kwan & Valdez 1983) while others have argued that GMCs form primarily from atomic gas through instability or large-scale shocks (Blitz & Shu 1980). A viable mechanism by which this could occur is the formation of convergent flows induced by a passing spiral arm (Ballesteros-Paredes, Vázquez-Semadeni & Sclo 1999). Of course, both modes of formation may occur: in high-density regions, where the vast majority of hydrogen is molecular it seems likely that molecular clouds form from the coagulation of smaller clouds, whereas in the outskirts of galaxies where the gas is predominantly atomic the compression of gas in spiral density shock waves provides a more plausible formation mechanism.

Observationally, star formation in discs seems to occur only above a given surface density threshold (Kennicutt 1989), with star formation dropping abruptly below the threshold even though the gaseous disc may extend far beyond it. Schaye (2004) describes a model in which this threshold arises naturally due to the thermal instability when gas cools from 10^4 K to the cold phase ($\sim$100 K), rendering the disc gravitationally unstable on a range of scales. This suggests that a combination of thermal instability and large-scale dynamics may be responsible for determining when and where GMCs form.

Elmegreen (2000) discusses observational evidence that GMCs are in fact short-lived entities that form, make stars and disperse again on their dynamical time-scale. This short time-scale alleviates the need for an internal energy source to sustain the observed internal supersonic turbulence, something that had puzzled astronomers for a long time. Pringle, Allen & Lubow (2001) discuss this assumption in more detail and suggest that GMCs form from agglomeration of the dense phase of the ISM, already in molecular form, when compressed in a spiral shock. They envisage the pre-existing molecular gas to be in dense 'wisps', in the interarm regions, formed from atomic gas by shocks, as simulated by Koyama & Inutsuka (2000).

Recent numerical simulations support the view that when clumpy gas is overrun by a density wave it produces structures that resemble GMCs. Wada, Meurer & Norman (2002) present high-resolution two-dimensional simulations of the evolution of perturbations in a cooling, self-gravitating disc in differential rotation. They show that the disc develops stationary turbulence, even without any stellar feedback. Bonnell et al. (2006) and Dobbs & Bonnell (2006) performed three-dimensional simulations of the passage of clumpy cold gas through a spiral shock. Their simulations produce dense clouds, with large internal velocity dispersion, reminiscent of the 'supersonic turbulence' seen in GMCs. They noted that the velocity dispersion is generated on all scales simultaneously, in contrast to what is usually meant by turbulence where energy cascades from large to small scales. Mac Low & Klessen (2004) review the current state of the art in simulations and models of GMC formation, including references to more recent work. In this picture of clouds, GMCs are temporary structures formed and dissolving in converging flows. They do not require an internal source of energy, are not in virial or pressure equilibrium and need not even be gravitationally bound. They point out that the relative contribution of galactic rotation and stellar sources to driving the observed turbulence is not clear.

2.3 Star formation in molecular clouds

In the older picture of cloud formation, GMCs were long-lived, gravitationally bound, virialized objects. The presence of supersonic turbulence ensures that clouds do not immediately collapse to form stars, as this would predict an SFR for the MW which is far higher than that observed. Locally unstable clumps collapse to form protostars, which built up their mass to produce the initial mass function (IMF) through competitive accretion (e.g. Bonnell et al. 1997).

However, simulations show that the energy contained in supersonic motions is quickly dissipated even in the presence of magnetic fields (see references in Mac Low & Klessen 2004). To sustain the turbulence therefore requires an energy source, for example, from star formation, yet some clouds have turbulence but no current star formation.

The modern picture is one in which clouds are short-lived structures and the turbulence results from the same process that formed the cloud in the first place. Observationally, GMCs turn a small fraction $\epsilon_\star \approx 0.1$ of their mass into stars before they disperse again. This low star formation efficiency of clouds may be due to the fact that they are short lived. The short lifetimes of (star-forming) clouds also follow from the small age spread in star clusters (see e.g. Gomez et al. 1992), and indicates that star formation in a given cloud only lasts for a few million years. The short lifetimes of GMCs then also suggests that competitive accretion (e.g. Bonnell et al. 1997) is less important in shaping the IMF (Padoan & Nordlund 2002).

Turbulence generates a range of substructures inside a GMC, and Padoan & Nordlund (2002) suggest that such 'turbulent fragmentation' builds a mass spectrum of proto-cores, some of which will collapse under their own gravity to form stars. The resulting IMF is a power law due to the self-similar nature of the turbulence. Only cores dense enough so that self-gravity can overcome their magnetic and thermal energy can collapse. This consideration flattens that IMF at low masses, and prevents very low-mass cores from forming stars. They also argue that the maximum mass is a fraction of the overall cloud mass.

A young stellar population does, of course, dump a lot of energy into its surroundings through stellar winds, ionization, and SN explosions. Even if these do not drive the observed turbulence, they may contribute to the destruction of the cloud, and prevent further star formation. Most simulations use such feedback from star formation to regulate the SFR.

[1] http://www.alma.nrao.edu/.

2.4 Summary

The current theory of star formation in disc galaxies suggests that supersonic turbulence, generated by a combination of galactic rotation and SNe, regulates the formation of proto-stellar cores inside more massive molecular clouds. Some fraction of these clouds can form stars, before the cloud itself is destroyed, by a combination of stellar feedback and the turbulence that built the cloud in the first place. The cooling of the cores to temperatures $\leqslant$100 K is dominated by grains and C II fine-structure lines and is opposed by photoelectric heating from small grains and polycyclic aromatic hydrocarbons, see Wolfire et al. (1995).

A numerical implementation of these processes requires high resolution to model the interstellar turbulence and follow the contraction of cores of masses a few $M_\odot$ at densities above 1 particle per cm^3. Such challenging simulations may be feasible in the near future for high-redshift galaxies but are not possible yet for $z = 0$ galaxies. Below we describe a model of cloud formation that tries to incorporate some of these processes with some simple rules.

We would like to apply the same rules to cosmological simulations of galaxy formation, which clearly requires a leap of faith. High-redshift galaxies may not have a well-defined disc, and hence the properties of the supersonic turbulence and the GMCs may well be very different. In the high-redshift simulations of Abel, Bryan & Norman (2000), the first molecular cloud is close to hydrostatic equilibrium, with pressure support slowly leaking away as it cools through molecular hydrogen line emission. This quasi-static evolution, reminiscent of a cooling flow, is very different from the dynamic turbulent fragmentation envisaged in the MW, with corresponding large differences in the predicted IMF. Furthermore, if the properties of the GMCs were similar, the behaviour of the cores may still be very different, with the reduced grain and metal cooling at higher z, making for a different IMF.

Despite these difficulties we must start somewhere. The assumption that the physics of the ISM (and therefore the stellar IMF) is similar at redshift zero and in the high-redshift universe is common in the simulation community. The understanding gained through these necessarily simplified simulations will allow us, over time, to investigate the physics relevant to galaxy formation at higher redshift.

3 DETAILS OF THE MODEL

As demonstrated in Section 1, in typical simulations of galaxy formation we can resolve the Jeans length of the ambient gas phase and so treat its hydrodynamic properties consistently. However, we cannot yet resolve the properties of the cold molecular phase of the ISM. We therefore follow the evolution of the ambient gas phase using a hydrodynamic simulation code, whereas we treat the cold phase using a statistical model that encapsulates the physics relevant to the formation and evolution of molecular clouds. In this section, we introduce the properties of the sticky particle model and describe the physics we have implemented.

Following Efstathiou (2000) we consider the ISM to consist of warm and hot ambient materials, and cold molecular clouds. We additionally treat the properties of SN remnants. Throughout this paper, the properties of the ambient medium will be represented with the subscript 'h', the properties of the molecular clouds with the subscript 'c', and the properties of the gas internal to SN remnants, or hot bubbles, with the subscript 'b'.

The ambient gas phase is represented using the entropy-conserving, parallel Tree-SPH code GADGET2 (Springel, Yoshida & White 2001; Springel 2005), which is a Lagrangian code used to calculate gravitational and hydrodynamic forces on a particle by particle basis. SPH was originally introduced by Lucy (1977) and Gingold & Monaghan (1977) (see e.g. Monaghan 1992 for a review). We will refer to the gas component treated using SPH as ambient gas to distinguish it from the cold molecular gas. Ambient gas at temperatures around 10^4 K will be referred to as 'warm', and gas at temperatures of 10^6 K and higher will be called 'hot'. We will see that in galaxy formation simulations, this ambient (i.e. non-molecular) medium naturally develops three relatively well-defined phases: a warm ($T \sim 10^4$ K) component in a galactic disc, a hot ($T \sim 10^6$ K) tenuous component of shock-heated gas in the halo, and a similarly hot component resulting from gas heated by SNe. The fourth, cold ($T \sim 100$ K) and molecular cloud phase is represented with sticky particles, which interact gravitationally with all other material in the simulation and are allowed to stick together forming more massive sticky particles. Stars and DM are both treated as collisionless particles by GADGET2.

The different phases of the ISM may interact with each other as follows: thermally unstable ambient gas may collapse into molecular clouds via thermal instability (Section 3.1). Molecular clouds can interact with each other to form GMCs (Section 3.2). GMCs then collapse into stars (Section 3.3). Stars disrupt the cloud they formed from and may, via SN feedback, return energy (Section 3.4.1) to the ambient phase. Hot bubbles blown by SNe can evaporate cold clouds (Section 3.5) and heat the ambient medium.

Fig. 1 contains a summary of all of the physics implemented in our model. The arrows represent a transfer of mass and/or energy from one phase to another. The distinction between clouds and GMCs is somewhat arbitrary; they are separated in the figure to allow for an easy pictorial representation of mass transfer within a single phase. Appendix A contains a list of frequently used symbols and their meaning.

Each physical process will be treated in turn in the remainder of this section. We first introduce the physics relevant to each physical process before discussing the numerical implementation. We will

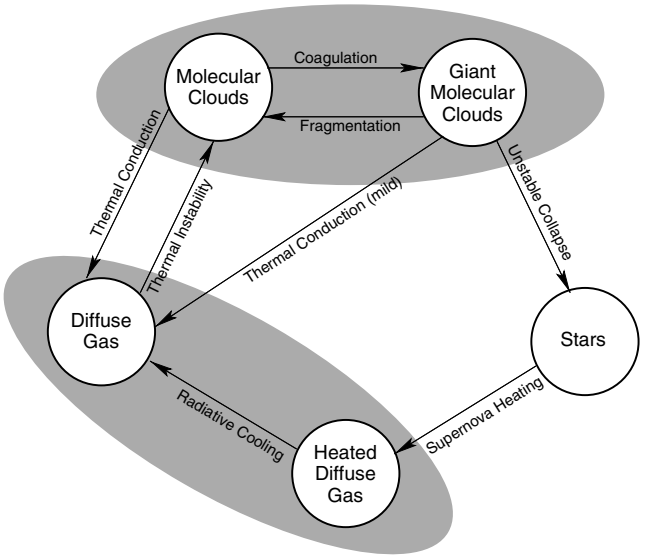

Figure 1. Summary of the physical processes that operate in our model of a two-phase ISM. The boundaries between molecular clouds and GMCs and between heated and non-heated diffuse gas are somewhat arbitrary and they are separated out in this figure only to highlight the different physical mechanisms that are operating at any given time.

also give our preferred physical values for the various parameters that occur. How we choose these is discussed in Section 4.

3.1 Radiative cooling and the formation of molecular clouds

Begelman & McKee (1990) show that under appropriate physical conditions, a thermal instability may operate in the ambient gas, which causes a fraction of the gas to condense into much colder molecular clouds. The sticky particle star formation prescription contains a basic representation of this process, based on a detailed treatment of baryonic radiative cooling.

3.1.1 Relevant physics

The radiative processes that we take into account are Compton cooling off the microwave background, thermal Bremsstrahlung cooling, line cooling and photoionization heating from hydrogen, helium and metal species in the presence of an imposed ionizing background. These routines were developed for a different project and will be described elsewhere.[2] Briefly, they use tabulated rates for radiative cooling and photoionization heating for many species and ionization states computed assuming ionization equilibrium using CLOUDY (version 05.07 of the code last described by Ferland et al. 1998) with a UV background given by Haardt & Madau 2001). The rates are tabulated element by element and we will assume solar abundance ratios and specify a fixed metallicity of the gas in solar units. We do, however, note that the behaviour of the system may depend on precisely which value of the metallicity we choose, and investigate this in Section 5.3

Other processes such as cosmic ray heating, and cooling by dust and atomic lines that affect the molecular gas in clouds are not treated explicitly since we do not model the internal properties of the clouds themselves.

We include a simple model to determine the rate at which the ambient gas forms molecular clouds. When we identify ambient gas that is thermally unstable (Begelman & McKee 1990), we allow it to collapse into molecular clouds. The rate at which this process occurs is goverened by the rate at which the gas is losing thermal energy by radiative cooling.

3.1.2 Numerical implementation

Following Yepes et al. (1997) we define a density threshold, $\rho_{\rm th}$, to determine when gas becomes thermally unstable. Gas with $\rho < \rho_{\rm th}$ undergoes ordinary radiative cooling. Gas with density above the threshold becomes thermally unstable and begins to be converted to molecular clouds. In addition to the density criterion we add a maximum temperature ($T_{\rm th}$) for gas to be called thermally unstable which has the effect of preventing SN-heated gas in dense regions from collapsing straight to the cold phase.

When gas has been identified as thermally unstable, it begins to form molecular clouds at a rate controlled by the rate at which the gas can lose thermal energy by radiative cooling:

$$\frac{{\rm d}\rho_{\rm c}}{{\rm d}t} = -\frac{{\rm d}\rho_{\rm h}}{{\rm d}t} = \frac{1}{u_{\rm h} - u_{\rm c}} \Lambda_{\rm net}(\rho_{\rm h}, u_{\rm h}), \quad (1)$$

where u represent an internal energies per unit mass. The subscripts 'h' and 'c' refer to the ambient phase (either warm or hot) and cold phase, respectively. $\Lambda_{\rm net}$ is the cooling rate of the ambient gas (erg cm^{-3} s^{-1}). We assume that the cold clouds remain at a fixed temperature of $T_{\rm c} = 100$ K and hence their thermal energy $u_{\rm c}$ is a constant as well.

In practice, each ambient gas particle is identified as either thermally unstable or non-thermally unstable. Non-thermally unstable gas undergoes radiative cooling; thermally unstable ambient gas forms molecular clouds at a rate controlled by the radiative cooling rate, as described by equation (1).

In this way each ambient gas particle can keep track of what fraction of its mass is in the form of molecular clouds. Gas in the molecular phase is ignored for the purposes of the SPH calculation. When the amount of mass in the molecular phase in a particle reaches the resolution limit of the simulation, a separate 'sticky particle', representing many sub-resolution molecular clouds, is created. This process decouples the molecular clouds from the associated ambient phase. Since we cannot resolve the individual molecular clouds in each sticky particle we work with the mass function of clouds. Initially we assume that the molecular clouds formed through instability are all in the smallest mass bin, that is that the clouds formed by thermal instability are very small, and will interact to form more massive clouds. In the following section, we describe the behaviour and evolution of the sticky particles in the simulation.

3.2 Cloud coagulation and GMC formation

Molecular clouds are typically many orders of magnitude more dense than the medium they form in MO77, and their behaviour is governed by a different set of rules than the ambient medium. This section describes the physics of the simplified molecular clouds in the sticky particle model and how it is implemented.

3.2.1 Relevant physics

We assume that clouds may be treated as approximately spherical objects that obey a power-law relation between mass ($M_{\rm c}$) and radius ($r_{\rm c}$):

$$r_{\rm c} = \left(\frac{M_{\rm c}}{M_{\rm ref}}\right)^{\alpha_{\rm c}} r_{\rm ref} = 36 \left(\frac{M_{\rm c}}{10^5\ {\rm M}_\odot}\right)^{0.3} {\rm pc}. \quad (2)$$

Here, $\alpha_{\rm c}$ describes how clouds grow as mass is added to them (if they remain at constant density then $\alpha_{\rm c} = 1/3$), and $M_{\rm ref}$ and $r_{\rm ref}$ are a reference mass and radius used to fix the normalization of this relation. The lower bound on molecular cloud masses is typically calculated to be 100 M$_\odot$ (Monaco 2004) due to the efficient destruction of smaller molecular clouds by photoionization. We introduce an upper limit by converting molecular clouds with large masses into stars (see Section 3.3 for discussion). In order to facilitate easy estimates of the relative importance of various effects, we have substituted typical numbers and units into most of the equations in this section.

3.2.2 Numerical implementation

Each sticky particle represents numerous cold clouds. Sticky particles are hydrodynamically decoupled from the ambient SPH phase of the gas and interact only gravitationally with the other phases in the simulation. However, when two sticky particles collide they may coagulate to form a more massive sticky particle. The mass

[2] We would like to thank our colleagues J Schaye, C Dalla Vecchia and R Wiersma for allowing us to use these rates.

of the smallest molecular clouds is typically orders of magnitude below the mass resolution in a cosmological simulation. We represent an entire mass spectrum of clouds statistically inside each sticky particle. Our formalism to treat the evolution of the mass function of clouds internal to each of the 'multiple cloud' particles will start from the Smoluchowski equation of kinetic aggregation (Smoluchowski 1916), which describes the behaviour of a system consisting of ballistic particles that can interact via mergers. The coagulation behaviour of this system is driven by a coagulation kernel, $K(m_1, m_2)$, that represents the formation rate of clouds of masses $m = m_1 + m_2$,

$$K = \langle \Sigma v_{\rm app} \rangle_v, \tag{3}$$

where $v_{\rm app}$ is the relative velocity of the clouds and Σ is the collision cross-section. For a Maxwellian distribution of velocities with three-dimensional dispersion σ we obtain $\langle v_{\rm app} \rangle = 1.3\sigma$ (Lee & Nelson 1988). The product of the approach velocity and the collision cross-section is averaged over the distribution of relative velocities. The cross-section is

$$\Sigma \approx \pi (r_{\rm c} + r'_{\rm c})^2 \left(1 + 2G \frac{M_{\rm c} + M'_{\rm c}}{r_{\rm c} + r'_{\rm c}} \frac{1}{v_{\rm app}^2} \right), \tag{4}$$

where the first term represents the collision geometric cross-section and the second term represents the effect of gravitational focusing (Saslaw 1985). The focused term becomes significant when the approach velocity is not much larger than the internal velocity dispersion of the system. In most cases of interest, the geometric term will dominate so the focused term is neglected. In these calculations, we need to assume that molecular clouds, although transient and turbulent, are stable for long enough for coagulation to take place. This is reasonable because the cloud velocity dispersion is typically larger than the sound speed of the cold cloud gas (Monaco 2004).

To model the cooling of sub-resolution molecular clouds via gravitational interaction it has been assumed that when molecular clouds with relative velocities, $v_{\rm app}$ greater than $v_{\rm stick}$ (a parameter in our simulations) collide they do not merge, but rather bounce back with relative velocity a fraction, η, of the initial approach velocity. Clouds with relative velocities less than $v_{\rm stick}$ merge. For simplicity it has been assumed that the velocity distribution of clouds is Maxwellian with a velocity dispersion that is a function of cloud mass, $\sigma = \sigma(m)$.

The upper and lower bounds on the molecular cloud mass function are set such that the smallest mass bin is comparable with the smallest clouds was can observe, and the largest molecular clouds are approximately the same mass as the largest clouds in the MW. The mass function is discrete. All clouds are assumed to form at the lowest mass, $M_{\rm min}$, and then the mass of each bin is a multiple of this value. This discrete mass function is neccessary when working with the Smoluchowski equation.

In order for us to be able to hold a mass function with a large number of bins internal to every single sticky particle without the requirement to store one number for each mass bin, we parametrize the mass function as a third order polynomial, and store only the four coefficients between time-steps.

As these sub-resolution clouds interact and merge, the one-dimensional velocity dispersion $\sigma(m)$ changes, which affects the rate of evolution of the cloud mass function, $n(m)$. Let $E_m = 3/2\, m\sigma^2(m)$ denote the random kinetic energy of clouds with mass m. The one-dimensional velocity dispersion is related to the three-dimensional velocity dispersion by $\sigma_{\rm 1D} = \sigma_{\rm 3D}/\sqrt{3} E_m$ and may change due to the following three distinct processes.

(i) Clouds with masses m' and $m - m'$ merge to form extra clouds of mass m, increasing E_m at a rate $\dot{E}_{\rm gain}$.

(ii) Clouds with masses m may merge with clouds of any other mass decreasing the number of clouds of mass m. This process decreases E_m at a rate $\dot{E}_{\rm loss}$.

(iii) Clouds with mass m may interact collisionally with clouds of any other mass and so lose kinetic energy. This process decreases E_m at a rate $\dot{E}_{\rm cool}$.

The net change in kinetic energy for particles of mass m during some time-step Δt is given by

$$\Delta E_m = \frac{{\rm d}E_m}{{\rm d}t} \Delta t = [\dot{E}_{\rm gain} - \dot{E}_{\rm loss} - \dot{E}_{\rm cool}] \Delta t, \tag{5}$$

and for this change in kinetic energy, the corresponding change in velocity dispersion is given by

$$\dot{\sigma} = \frac{2\dot{E} - \dot{M}\sigma^2}{2M\sigma}. \tag{6}$$

Details of the equations used to model these processes are given in Appendix B, and the method by which they are solved numerically in Appendix C.

The same processes (cooling and merging) are followed explicitly for the individual particles in our simulations, which can interact in the same two ways as the unresolved sub-resolution clouds by merging to form more massive sticky particles or cooling to decrease their relative velocities. Following the same rules should allow us to remove much of the resolution dependence of the star formation prescription. As the mass resolution of a simulation is degraded, more massive clouds will be treated with the sub-grid physics; our implementation should ensure that the large-scale results are approximately the same. This is demonstrated in Section 4.1.2.

3.3 Cloud collapse and star formation

The vast majority of stars form in GMCs. This process is described in the sticky particle model by allowing for the most-massive clouds in the galaxy to collapse into stars.

3.3.1 Relevant physics

We follow the process of star formation in our simulations by waiting for star-forming clouds to be created by the coagulation process described in Section 3.2. We define star-forming clouds to be clouds of a mass similar to the most-massive clouds observed in the MW ($\sim 10^6$ M$_\odot$). When one of these star-forming clouds is created, it is assumed to collapse on a short time-scale and approximately $\epsilon_\star \sim 10$ per cent of its mass is converted into stars, whilst the remainder is disrupted by stellar feedback processes including stellar winds, SN feedback and photoionization. This process reflects that although stars may form in less-massive molecular clouds, it is not until the relatively rare, massive O and B stars are created that the cloud is destroyed (Elmegreen 1983).

We assume that each cloud collapse forms a single stellar population with an IMF of the standard Salpeter (1955) form

$$N(M)\, {\rm d}M \propto M^{-(1+x)}\, {\rm d}M, \tag{7}$$

where x is the slope of the IMF and takes the usual value of 1.35. The masses of stars are assumed to lie between well-defined minimum and maximum values, $M_{\star,\rm min}$ and $M_{\star,\rm max}$.

© 2007 The Authors. Journal compilation © 2007 RAS, MNRAS **376,** 1588–1610

3.3.2 Numerical implementation

The treatment of star formation adopted in most simulations is to identify gas that is likely to be star forming and impose an SFR given by the Schmidt law,

$$\dot{\rho}_\star = C\rho_{\rm gas}^{N_{\rm SF}}. \tag{8}$$

Here, $\dot{\rho}_\star$ and $\rho_{\rm gas}$ denote the rate of star formation per unit volume and the gas density, respectively. This power-law relation between SFR and gas density was found to hold over many orders of magnitude by Kennicutt (1998), who constrained the exponent to be $N_{\rm SF} = 1.4 \pm 0.2$.

We take a different approach: unstable molecular clouds are identified in the simulations as any cloud with a mass greater than $M_{\rm sf}$. We identify the formation of these massive clouds by using the cloud mass function, as stored internally to every single sticky particle. These unstable clouds are assumed to collapse on a very short time-scale, forming stars.

As soon as a cloud of mass $M_{\rm sf}$ forms, it is assumed to be disrupted by OB stars on a time-scale of $\sim$10 Myr (Matzner 2002), the rest of the massive cloud is broken down into smaller clouds and the coagulation process begins all over again as described in Section 3.2. This process is modelled by taking the fraction of the cloud 's mass that does not turn into stars, $1 - \epsilon_*$, and assuming that the net effect of the stellar feedback processes is to fragment the GMC into the smallest clouds represented in the sticky particle internal mass function. This has the net effect of steepening the cloud mass function.

Each star particle formation event represents the formation of a single stellar population of stars that are all assumed to have the same age, and to be drawn from the Salpeter IMF. Each stellar particle is therefore formed with a mass approximately equal to ϵ_* times the mass of a starforming cloud. If this particle mass is not allowed by the mass resolution of a given simulation, then we either store up unresolved stars internal to a sticky particle (if the star mass is too small to be allowed) or split it into multiple, equal mass particles (if the star mass is too large to be allowed).

3.4 Supernova feedback

Our simulations include only energy feedback from type II SNe (SNeII). These events return energy from the stars to the ambient phase. We note that it is not currently computationally feasible to resolve the properties of SN remnants so we treat them with a simple, analytic prescription. The mechanism by which SN feedback is implemented in our model is discussed here.

3.4.1 Relevant physics

Each star of mass greater than 8 $\rm M_\odot$ releases $10^{51}\,E_{51}$ erg in thermal energy when it undergoes an SN event. The lifetime, t, of a star of mass M (where $M > 6.6$ $\rm M_\odot$) is given by (Padovani & Matteucci 1993):

$$\frac{t}{\rm Gyr} = 1.2\left(\frac{M}{\rm M_\odot}\right)^{-1.85} + 0.003. \tag{9}$$

Each SN explosion can be approximated as the injection of energy at a single point in space. If we assume that the ambient density on scales of interest is approximately homogeneous, with density $\rho_{\rm h}$, then each SN explosion can be modelled as a Sedov blast wave (Sedov 1959). According to this solution, if at time $t = 0$ we release an amount of energy $E_{\rm b}$, then after time t the resulting blast wave will have reached a radius $r_{\rm b}$ given by

$$r_{\rm b} = \left(\frac{E_{\rm b}}{\rho_{\rm h}}\right)^{1/5} t^{2/5}$$
$$= 292\left(\frac{E_{\rm b}/10^{51}\ {\rm erg}}{\rho_{\rm h}/0.1\,{\rm cm^{-3}}}\right)^{1/5}\left(\frac{t}{10\ {\rm Myr}}\right)^{2/5}{\rm pc}. \tag{10}$$

These hot SN bubbles have two main effects. First, as they expand and decelerate the SN-heated gas will get mixed in with the surrounding ambient medium; the net result of this process is the heating of the ambient medium. Secondly, as discussed in Section 3.5, any cold clouds caught inside an SN bubble will undergo evaporation.

There are two main assumptions that must hold for the Sedov solution to be valid, the pressure of the ambient medium, and the cooling rate inside the bubble, must both be negligible. Often at least one of these assumptions is invalid. If the ambient medium has a low density and is very hot, for example, due to a previous set of explosions, then its pressure is no longer negligible and the Sedov solution breaks down. If the ambient medium is dense, then radiative cooling becomes an important process. In the remainder of this section, we describe various modifications to the standard Sedov solutions, which allow us to model SN remnants in a wider variety of conditions.

In the case of a hot, tenuous medium, the radius of each blast wave is increased (Tang & Wang 2005). These authors derived a fitting formula for the velocity of an SN blast in a hot medium, which is accurate to within 3 per cent:

$$r_{\rm b}(t) = \int_0^t c_{\rm h}\left(\frac{t_{\rm c}}{t'}+1\right)^{3/5}{\rm d}t', \tag{11}$$

$$= 156\int_0^{t/{\rm Myr}}\left(\frac{t_{\rm c}}{t'}+1\right)^{3/5}{\rm d}t'\ {\rm pc}, \tag{12}$$

where $c_{\rm h}$ is the sound speed of the ambient medium. We assumed a temperature of $T_{\rm h} = 10^6$ K, mean molecular weight of $\mu = 0.58$, blast wave energy of 1×10^{51} erg and an ambient density of 0.1 atoms per cm^3 in order to illustrate the order of magnitude of $r_{\rm b}$:

$$t_{\rm c} = \left[\left(\frac{2}{5}\xi\right)^5\frac{E_{\rm b}}{\rho_{\rm h}c_{\rm h}^5}\right]^{1/3}$$
$$= 0.012\left[\left(\frac{\xi}{1.14}\right)^5\frac{E_{\rm b}/10^{51}{\rm erg}}{(\rho_{\rm h}/0.1\,{\rm cm^{-3}})(T_{\rm h}/10^6{\rm K})^{5/2}}\right]^{1/3}{\rm Myr}, \tag{13}$$

where $t_{\rm c}$ is a characteristic time, and ξ equals 1.14 for a gas with adiabatic index $\gamma = 5/3$. This solution matches the standard Sedov evolution, $r_{\rm b} \propto t^{2/5}$, closely until $t \sim t_{\rm c}$, after which the shell 's velocity becomes constant, $r_{\rm b} \propto t$. This modification allows us to take into account that the majority ($\sim$90 per cent) of SNeII happen in preheated SN bubbles (Higdon, Lingenfelter & Ramaty 1998) and, therefore, the approximation that the pressure of the ambient medium is negligible is often incorrect. Fig. 2 shows the difference between an adiabatic gas SPH simulation of an SN-induced shockwave, the pure Sedov solution and the blast wave radius as predicted by the hot medium modified Sedov solution from Tang & Wang (2005).

Situations where radiative cooling are important may be taken into account using the prescription of Thornton et al. (1998), whose high-resolution simulations of SN explosions expanding in an ambient

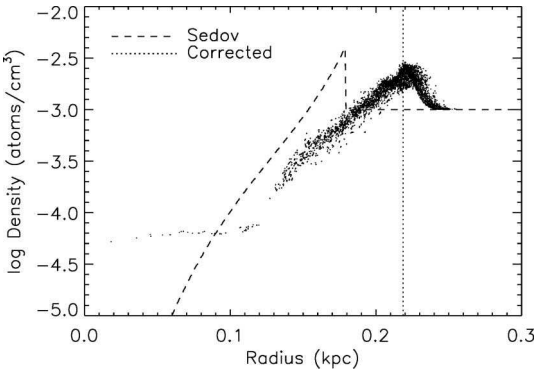

Figure 2. Comparison between SPH simulation of a Sedov blast, the Sedov solution and the hot medium correction of Tang & Wang (2005). The points represent individual SPH particles, the dashed line is the Sedov solution and the dotted line is the blast wave radius as calculated with the hot medium correction. The initial condition had a density of 0.001 atoms per cm^3 and a temperature of 10^6 K. 10^{51} erg was injected to the central 32 particles at t_0. This plot was made after the blast wave had evolved for 0.3 Myr.

medium with temperature $T_h = 10^3$ K, provide the total thermal energy in SN bubbles as a function of time, ambient density and metallicity. We perform bilinear interpolation on the results in tables 2 and 4 of Thornton et al. (1998) to obtain the SN bubble radius and thermal energy at any given time.

Neither of these solutions treats the more general case of SN remnant expansion in a porous ISM, which may have regions of both high and low ambient density, and so we are not able to include the effects of SNe fully self-consistent. In most of our simulations, we use the simple Sedov solution for the evolution of the SN blast waves, but note that the details of our prescription are uncertain. In Section 5.3, we investigate the effects of using different implementations of the blast wave implementation to estimate how important the details of the behaviour of SN remnants are to the overall properties of the galaxy. Both the radiative cooling and blast wave velocity physics are varied.

3.4.2 Numerical implementation

By assuming that each stellar particle in the simulation represents an entire population with the same age we can calculate the minimum and maximum masses of stars that undergo SN events over any given time period using equation (9). Each of these SNe is assumed to go off in a neighbouring gas particle (i.e. one for which the distance, r, to the star is smaller than its smoothing length, h, in the SPH formalism). We chose this particle randomly from the neighbours, with a weight computed from the solid angle, Ω, it subtends on the sky as seen from the position of the star particle:

$$\Omega = 4\pi \left[1 - \frac{r}{\sqrt{(r^2 + h^2)}}\right]. \quad (14)$$

This weighting forces that nearby hot, diffuse gas (which tends to have larger h, hence larger weight) is heated more frequently than cooler, denser parts of the ambient medium (which are dense, hence have smaller h).

We do not transfer all SN energy to gas particles each time-step. Assuming that SN explosions are distributed evenly in time and space we can calculate for every ambient gas particle a 'porosity' of SN bubbles, $Q = V_B/V_A$. For the volume associated with a gas particle we use $V_A = (4\pi/3)\,h^3$, and $V_B = (4\pi/3)\sum r_b^3$ is the total volume of all the SN bubbles in this particle. When Q is greater than a critical value, $Q_{crit} \approx 1$, the ambient phase is heated, else the available SN energy is carried over to the next time step. This ensures that the ambient phase is only heated when hot SN bubbles make up a significant fraction of the volume. There are two motivations for this, first, a given SPH particle cannot represent more than one phase at a given time, and secondly, simulations usually do not limit the time-step to be a fraction of the cooling time. Consider a warm, $T \sim 10^4$ K, SPH particle in the disc. If a small amount of SN energy is injected into this dense particle, it will cool very efficiently since the cooling rate is very high. It is only when the particle is heated to $T \gg 10^6$ K that the reduced cooling may affect the particle dynamically, so that it will move into lower density gas, further decreasing its cooling rate, and becoming part of the hot, tenuous gas. Storing the available heating until the SN bubbles fill a significant fraction of the particle is a way of easing the transition from warm to hot and makes the outcome less dependent on the time-step.

To determine the porosity Q, we need to know the current radii, r_b, of SN bubbles. The radius r_b depends on the ambient gas properties and also on the available energy, E_b, as discussed in Section 3.4.1. Typically a single stellar particle will undergo multiple SN events over a single time-step. Using equations (9) and (10) and obtaining the SPH estimate of the ambient gas density at the position of the star particle, we can estimate the average radius of all SN bubbles blown by a given star particle at any time. Working under the assumption that the porosity of the ISM is low, we calculate the radiative loss from each bubble separately. When the porosity of the ISM becomes $Q > Q_{crit} \sim 1$, the SN bubbles are overlapping significantly and all coherent structure is assumed to be wiped out. The ambient gas particles are heated by the remaining thermal energy in the SN bubbles and they are considered to disperse. The porosity is set back to zero. Note that using the Sedov solution implies we neglect radiative cooling in the remnants to determine the porosity, Q. However, to determine how much energy is in the bubbles once we decide to heat the particle, we do use the tables of Thornton et al. (1998) to account for radiative cooling in the SN shells. We believe that even though this treatment is not fully consistent, it does capture the main physics.

3.5 Thermal conduction

Thermal conduction between the ambient and cold gas in the simulation is an important ingredient in the self-regulation of the SFR in our model of the ISM.

3.5.1 Relevant physics

Thermal conduction has two primary effects. The first is to smooth out the temperature and density profiles inside SN remnants. In the strong explosion solution of Sedov, where thermal conduction is neglected, the temperature of the blast wave increases sharply towards the centre of the blast. This is due to the fact that the gas near the origin was heated by a stronger shock than that at the edges and thereafter evolves adiabatically. The effect of thermal conduction is to efficiently transport heat from the centre of the blast to the outer cool regions. The temperature of the interior of the SN blast, T_b, is then approximately constant and equal to the mean temperature of the blast (MO77 Chevalier 1975):

$$\left(\frac{T_b}{10^8\ \mathrm{K}}\right) = 1.2 \left(\frac{r_b}{10\ \mathrm{pc}}\right)^{-3} \left(\frac{n_b}{0.1\ \mathrm{cm}^{-3}}\right)^{-1} \left(\frac{E_b}{10^{51}\ \mathrm{erg}}\right), \quad (15)$$

where n_b and T_b are the mean density and temperature inside the bubble, respectively. We assume r_b to be described by Sedov 's

self-similar solution. The density n_b is also approximately constant and is given in terms of the ambient density, n_h, as

$$\frac{n_b}{n_h} = 1 + x^{-5/3} \tag{16}$$

$$\equiv 0.65 \left(\frac{r_b}{10\ \mathrm{pc}}\right) \Sigma_{con}^{1/5} \left(\frac{n_h}{\mathrm{cm}^{-3}}\right)^{3/5} \left(\frac{E_b}{10^{51}\ \mathrm{erg}}\right)^{-2/5}. \tag{17}$$

The dimensionless number Σ_{con} represents the effectiveness of evaporation,

$$\Sigma_{con} = \frac{\alpha_{con}}{3} \left(\frac{r_c}{\mathrm{pc}}\right)^2 f_{cl}^{-1} \phi^{-1}, \tag{18}$$

(McKee 1977), and depends on $\alpha_{con} = \dot{r}_b/c_h$ (the ratio of the velocity of the SN blast wave to the sound speed of the medium), the cloud 's radius, r_c, the volume filling factor of the cold clouds, f_{cl}, and the efficiency of thermal conduction, ϕ (see MO77 for details). For a pure Sedov blast wave $\alpha_{con} = 1.68$. The presence of magnetic fields and turbulence may decrease ϕ below its maximum value of $\phi = 1$. We compute f_{cl} for each sticky particle from its current cloud mass spectrum, given the assumed cloud mass–radius relation, equation (2).

The second effect of thermal conduction is to evaporate cold clouds. According to (McKee 1977; Cowie 1977), the evaporation rate is well described by

$$\left(\frac{\dot{M}_c}{\mathrm{M}_\odot \odot \mathrm{Myr}^{-1}}\right) = -0.44 \times \left(\frac{T}{10^6\ \mathrm{K}}\right)^{5/2} \left(\frac{r_c}{\mathrm{pc}}\right). \tag{19}$$

3.5.2 Numerical implementation

Since we store the mass function of molecular clouds internal to each sticky particle explicitly (Section 3.2), we can apply equation (19) along with equation (2) to each cloud mass bin to calculate the total mass loss of a cloud over one time-step. The evaporation rate of the cloud depends on the temperature of the ambient gas, which is represented with SPH particles. However, as we discussed above, some fraction Q of the volume of each SPH particle may be filled by hot SN bubbles, in which the evaporation rate of clouds may be much higher. Since we have computed Q, we can take this important effect into account.

Consider a single molecular cloud in thermal contact with an ambient medium of (constant) temperature T. The mass of a cloud at the end of a time-step (M_f) is related to its mass at the start of the time-step (M_i) by

$$M_f = \left[M_i^{1-\alpha_c} - (1-\alpha_c) \frac{0.44 T^{5/2} r_{ref}}{M_{ref}^{\alpha_c}} \Delta t \right]^{1/(1-\alpha_c)}, \tag{20}$$

where T is in units of 10^6 K, masses are in $\mathrm{M}_\odot$, lengths are in pc and times are in Myr.

Equation (20) represents the mass-loss rate for a single cloud in contact with a medium of temperature T. More generally in a porous medium a single cloud of mass m has a mean mass-loss rate described by

$$\dot{M}_{cloud} = -Q \dot{M}_{bubble} - (1-Q) \dot{M}_{ambient}, \tag{21}$$

where $\dot{m}_{bubble}$ and $\dot{m}_{ambient}$ represent the rate of mass loss for a cloud inside an SN bubble and situated in the ambient medium, respectively.

Equation (20) can be applied directly to the evaporation of a cloud in the local ambient medium ($\dot{m}_{ambient}$). However, to apply the same formula to the evaporation of clouds inside SN bubbles we need to account for the fact that although the temperature inside the bubbles remains uniform, due to conduction, it is not constant in time, but decreases as the bubble expands. We therefore make the additional assumption that the mean temperature of the SN remnant is constant over a time-step (a good approximation after a short ($\sim$20 yr) transient phase). Under this assumption equation (20) can be applied successfully to the more general case of evaporation in a porous medium. Equations (19) and (20) are used to show that the total mass-loss rate for clouds of mass m in a volume V_A is given by

$$\left(\frac{\dot{M}_c}{\mathrm{M}_\odot\ \mathrm{Myr}^{-1}}\right) = -0.44 \left(\frac{M_c}{\mathrm{M}_\odot}\right)^{\alpha_c} \left(\frac{r_{ref}}{\mathrm{pc}}\right) \left(\frac{M_{ref}}{\mathrm{M}_\odot}\right)^{-\alpha_c} \left[Q \left(\frac{T_b}{10^6\ \mathrm{K}}\right)^{5/2} + (1-Q) \left(\frac{T_a}{10^6\ \mathrm{K}}\right)^{5/2} \right]. \tag{22}$$

Under the assumption that T_b, the mean temperature of SN remnants, and T_a, the mean ambient temperature, are constant over any single time-step we can write

$$\left(\frac{\dot{M}_c}{\mathrm{M}_\odot\ \mathrm{Myr}^{-1}}\right) \equiv \lambda \left(\frac{M_c}{\mathrm{M}_\odot}\right)^{\alpha_c}. \tag{23}$$

In order to calculate the constant of proportionality, λ, we use an estimate of the mean temperature and density inside an SN remnant. These estimates were obtained by noting that by definition $Q \equiv V_B/V_A$. (V_B and V_A represent the total volume in bubbles and the ambient phase, respectively.) The mean radius of an SN remnant is then

$$r_b = \left(\frac{3 Q V_A}{4\pi N_{SN}}\right)^{1/3}, \tag{24}$$

where N_{SN} is the total number of SN explosions that have affected the local ambient medium (calculated from equations 9 and 7). The mean density inside the SN remnants, n_b, may then be calculated from equations (16) and (17) and the mean temperature from equation (15).

Over a period of time Δt a cloud with mass M_I will evaporate to a mass of M_F, given by

$$M_F = \left[M_I^{(1-\alpha_c)} - \lambda \Delta t \right]^{1/(1-\alpha_c)}. \tag{25}$$

Thermal conduction efficiently destroys smaller clouds, but its effects are far less dramatic on larger clouds. Fig. 3 shows the evolution of an initially power-law mass spectrum of clouds in a hot medium. The energy used to evaporate a mass $M_F - M_I$ of cold clouds is removed from the SN remnants.

3.6 Mass resolution limits

The sticky particle model allows particles of all types to change their mass via processes including merging, thermal conduction and star formation. For this reason it is necessary for us to introduce numerical minimum and maximum masses on all particle types. We define at the initial time a characteristic mass resolution for our simulation, M_{char}, typically this is set equal to the mass of the ambient gas particles in the initial conditions. Where more than one mass of ambient particles is present (e.g. in the model galaxies discussed in Section 5), we use the mass of the gas particles that will be forming most stars. We then define minimum and maximum particle masses relative to this characteristic mass scale.

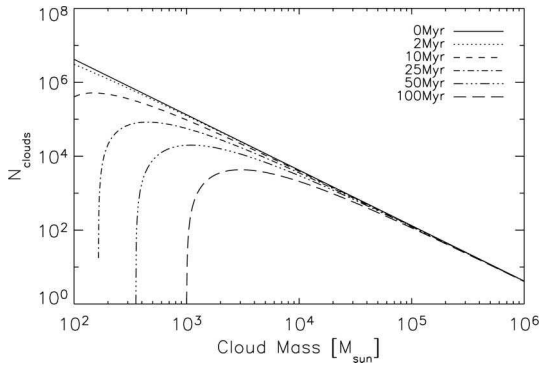

Figure 3. Evolution of a population of molecular clouds as they are evaporated by a hot ambient medium. The initial cloud mass function is a power law. The temperature of the ambient medium is assumed to be 10^5 K, the porosity of the medium is assumed to remain constant at 0.2, and the temperature of the SN remnants is $\approx 10^6$ K. Thermal conduction acts to preferentially destroy the smaller clouds.

Ambient gas particles may have their mass decreased by the formation of molecular clouds. If the total mass of a gas particle becomes less than $0.1M_{\rm char}$, then it is converted entirely into a cloud particle. The ambient gas particles may also have their mass increased by the process of thermal conduction. If a gas particle becomes more massive than $4M_{\rm char}$, then it is not allowed to grow any more, and the evaporated cloud mass is given to a different particle. In practice this limit is rarely, if ever, reached as evaporating cold clouds effectively cool the ambient gas particles so they become inefficient at thermal conduction.

Sticky particles may decrease their mass by star formation and evaporation. If the mass of a sticky particle drops below $0.1M_{\rm char}$, then it is either completely evaporated or completely converted into stars. Coagulation may drive the mass of a sticky particle to be very large. In practice this is not a real concern since when a sticky particle becomes very massive the rate at which its internal clouds coagulate also increases, causing it to form stars very rapidly.

Stars have a maximum and minimum mass of 4 and $0.1M_{\rm char}$. If a star forms with a mass greater than the maximum allowed mass, then it is split into a number of smaller star particles. A sticky particle may not form a star with a mass lower than the minimum allowed mass. In this eventuality, the mass of the 'unresolved' stars is tracked internally by the sticky particle and added into the next star formation event until the total mass of stars formed reaches the resolution limit of the simulation.

These particle mass limits keep all particle masses in the range $(0.1–4)M_{\rm char}$, which both minimizes two-body effects between very massive and very small particles and prevents the formation of very many low-mass particles, which are computationally very expensive to evolve.

4 PARAMETER ESTIMATION

The various physical processes in the star formation and feedback models have physical parameters associated with them. Before we discuss the properties of our model in detail we discuss how its free parameters can be constrained.

The free parameters that control the thermal instability and formation of the molecular clouds are $\rho_{\rm th}$ and $T_{\rm th}$, the physical density and temperature at which thermal instability is allowed to set in and radiative cooling creates molecular clouds. Wolfire et al. (1995) found that a diffuse ISM naturally settles into two stable phases, with a sharp cut-off between the ambient and molecular phases at a density of approximately 1 atom per cm^3. We use this as the value of $\rho_{\rm th}$. A threshold temperature $T_{\rm th} = 10^5$ K allows the gas in galaxies which cools radiatively to $\sim 10^4$ K to collapse into clouds but prevents SN-heated material (typically at temperatures of 10^6 K) from forming molecular clouds until it has radiated away most of its SN energy.

The properties of the molecular clouds themselves are contained in four parameters: $r_{\rm ref}$, $M_{\rm ref}$, and $\alpha_{\rm c}$ as defined in equation (2) and $u_{\rm c}$, the internal energy per unit mass of molecular clouds. The first three values are set by comparison with observations of molecular clouds in the nearby galaxy M33 (Wilson & Scoville 1990):

$$\left(\frac{r_{\rm c}}{\rm pc}\right) = (36 \pm 6)\left(\frac{M}{10^5\ {\rm M}_\odot}\right)^{0.3\pm0.1}. \quad (26)$$

Thus, $r_{\rm ref}$ and $M_{\rm ref}$ are assumed to be 36 pc and 10^5 M$_\odot$, respectively. This calibration (and an assumed $\alpha_{\rm c}$ of 0.3) suggests a radius of 122 $\pm$ 6 pc for the largest clouds observed in the MW (6×10^6 M$_\odot$ (Williams & McKee 1997).

The properties of the stars and associated feedback are contained within four parameters: x, the slope of the IMF, E_{51}, the energy of each SN blast in units of 10^{51}erg, $M_{\star,\rm min}$, the minimum star mass, and $M_{\star,\rm max}$, the mass of the largest allowed stars. For E_{51} we use the fiducial value of 1.0 noting, however, that the value of E_{51} is very uncertain and may be significantly higher. The effects of varying E_{51} are investigated in Section 5.3. For the purposes of this work, uncertainties in the IMF are neglected and x is assumed to take on the standard Salpeter value of 1.35. We follow Kawata & Gibson (2003) in adopting values 0.2 and 60 M$_\odot$ for the minimum and maximum stellar masses, respectively.

The star formation efficiency in a single cloud collapse is also somewhat uncertain and is known to be approximately $\epsilon_\star \approx 11$ per cent (Williams & McKee 1997) in the MW.

The thermal conduction efficiency is characterized by two numbers: $\alpha_{\rm con}$, the ratio of the blast wave velocity to the ambient sound speed and ϕ, the efficiency of thermal conduction. Following MO77, the value of $\alpha_{\rm con}$ is set to 2.5 (for the ideal Sedov blast wave case, $\alpha_{\rm con}$ is 1.68; the presence of thermal conduction changes this value). The thermal conduction efficiency parameter is assumed to be $\phi = 1$. The presence of magnetic fields and turbulence may change ϕ significantly; we investigate the effect of moving away from this value in Section 5.3

This leaves $v_{\rm stick}$ (the maximum relative cloud velocity for mergers) and η (the fraction of a cloud 's velocity lost per non-merger collision) as free parameters that are hard to constrain via observation. It is noted that the large-scale behaviour of a given simulation is largely independent of the value of η. This is because the cold cloud velocity dispersion is always limited by $v_{\rm stick}$. In the following section simple simulations are used in order to calibrate the properties of the physical model.

4.1 One-zone simulations

4.1.1 Simulation details

A 'one-zone model' is a periodic box that represents a fixed mass and volume (i.e. a static, periodic box with no mass outflow). The ambient ISM phase is assumed to be homogeneous. Initially, for a chosen mean density of matter we assume that 50 per cent of the material is initially in the hot phase at a temperature of $T_0 = 10^6$ K. The remaining gas is initially in cold clouds with an IMF that is a very steep $[N(M)\,{\rm d}M \propto M^{-8}\,{\rm d}M]$ power law. Numerically, we represent

© 2007 The Authors. Journal compilation © 2007 RAS, MNRAS **376,** 1588–1610

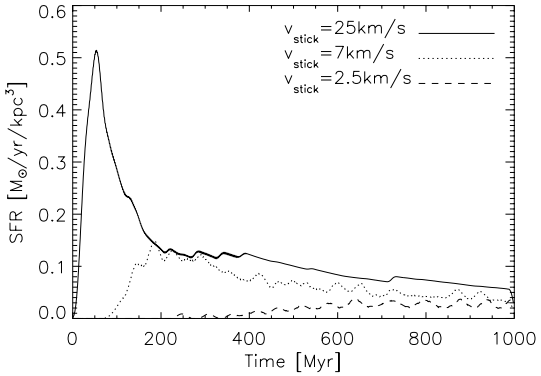

Figure 4. SFR as a function of time for a one-zone box with three different values of $v_{\rm stick}$. The initial gas density is $n_0 = 2$ cm^{-3} in each case. Each curve follows the same general shape; there is an initial delay during which the first GMCs are forming. The unopposed collapse of the first GMCs causes a burst of star formation, which is quickly regulated by the effects of feedback from stellar winds and SN explosions. After this initial burst the SFR in the simulation settles down and gradually decreases as the gas in the box is used up.

the different phases as follows: the ambient phase is assumed to be homogeneous and isotropic and so is represented by a single density and temperature throughout the whole periodic volume, molecular clouds are represented by discrete sticky particles that are spawned at a random point in the computational volume with a random velocity, and stars are not tracked individually, and are assumed to heat the whole volume evenly when they undergo SN explosions. The mass resolution of the molecular phase is approximately 10^7 M$_\odot$, although this figure is varied in Section 4.1.2

This initial situation represents hot, dense gas that has just begun to experience a thermal instability and started forming its first molecular clouds. The volume we simulate is 1 kpc^3. The hot phase will evaporate cold clouds through thermal conduction, and can cool via radiative processes using a simple tabulated cooling function from Sutherland & Dopita (1993) (assuming solar metallicity). Cold cloud particles are scattered randomly throughout the volume and given random velocities. Clouds do not feel gravitational forces. Depending on the parameters, the ambient phase will cool radiatively to form more molecular gas. Clouds will coagulate to form GMCs, which in turn form stars. The associated SNe evaporate smaller clouds, and may heat the ambient medium and quench the star formation. This sequence of events is plotted in Fig. 4; the same general shape is observed for each value of $v_{\rm stick}$; there is a brief delay as the first clouds coagulate to form GMCs; these clouds then collapse and form stars, which undergo SNe and quench the star formation. On a longer time-scale, the quiescent SFR slowly decreases as the available gas is consumed by stars. Since the dynamical equilibrium is reached on a very short time-scale, typically a couple of hundred Myr, we assume instantaneous recycling when considering SN feedback. The role of $T_{\rm th}$ is suppressed in the one-zone simulations, due to the fact that energy injected via SNe cannot escape the volume.

The lack of self-gravity does not affect the global properties of the volume significantly. From equation (4) assuming typical cloud properties ($M_{\rm c} \approx 10^5$ M$_\odot$, $r \approx 50$ pc) and a reasonable velocity dispersion ($\sigma_{\rm 1D} = 7$ km s^{-1}), the ratio of the geometric part of the cross-section to the gravitationally focused part is approximately 0.1; therefore, direct collisions between clouds account for the majority of the collisions and gravitational focusing makes for an effect of only 10 per cent. In the following section, we will choose a value of $v_{\rm stick}$ by comparing the SFRs in one-zone volumes with the Schmidt law, and also look at the properties of one-zone volumes.

As noted in Section 4 the properties of the simulation are largely independent of η. We assume a value of 0.5 throughout the rest of this paper.

4.1.2 Calibrating the base model

The one-zone model provides a useful sandbox in which we can investigate a wide variety of parameter choices in a relatively computationally inexpensive environment. In the following section, we discuss our choices for the values of the different parameters. The effects of moving away from this 'base model' are discussed more fully in later sections.

The parameters that are available for tuning the output of the model are as follows. The cold cloud reference size and radius ($r_{\rm ref}$, $M_{\rm ref}$); the slope of the cloud mass–radius relation, $\alpha_{\rm c}$; the efficiency of star formation in any given cloud collapse, $\epsilon_\star$; the maximum relative cloud velocity for merger ($v_{\rm stick}$); and the amount of energy ejected per SNII event (E_{51}).

Even though the initially assumed cloud spectrum, $N(M)\,{\rm d}M \propto M^{-8}\,{\rm d}M$, is very steep and far from equilibrium, SN feedback and cloud coagulation rapidly build a mass spectrum $N(M)\,{\rm d}M \propto M^{-\alpha}\,{\rm d}M$ with $\alpha \approx 2$ (Fig. 5), close to what is the observed cloud spectrum in the MW (dashed line) and M33 (dotted lines). This gives us confidence that, although the modelling of cloud formation is simple, it does produce a realistic cloud spectrum.

The ISM model can also reproduce the observed Schmidt law. We find that in our model the interaction between the coagulation of clouds and their destruction by stars leads to an SFR–density relation that is in good agreement with observation (Fig. 6) if $v_{\rm stick}$ is set to 7 km s^{-1}. This represents a reasonable value for the molecular cloud velocity dispersion, as considering theoretical models for the origin of random motion on molecular clouds, we would expect typical velocity dispersions in the range 5–7 km s^{-1} (Jog & Ostriker 1988).

The effect of changing the mass resolution of the simulation over two orders of magnitude is demonstrated in Fig. 7. Sub-resolution clouds that are simulated only by integrating the coagulation equations are designed to behave in exactly the same way as the resolved cloud particles in the simulation, and so we expect the simulations not to depend strongly on particle number. This is borne out by the good agreement between simulations carried out with only one

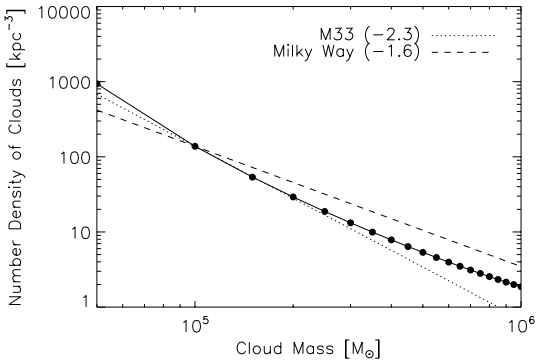

Figure 5. Mass function of clouds after 1 Gyr in a one-zone model. The dashed and dotted lines represent the slopes of the mass functions in the MW (Solomon et al. 1987) and M33 (Rosolowsky & Blitz 2004). The numbers in the legend represent the power-law slopes in each of the galaxies. It is clear that we obtain a good agreement between our model and the cloud mass spectrum in real galaxies.

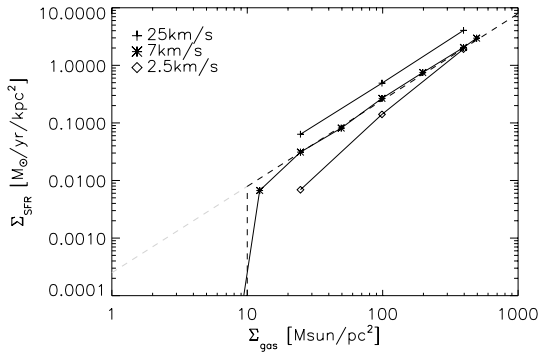

Figure 6. Schmidt law. The diagonal dashed line represents the observed star formation law (Kennicutt 1998) and the vertical line represents the observed cut-off in star formation ($10\,M_\odot\,pc^{-2}$; Schaye 2004). Each point represents the SFR averaged over a period of 500 Myr for a separate one-zone simulation. Data are shown for three different values of v_{stick}; the base value used in all subsequent simulations is $7\,km\,s^{-1}$. We calculate SFRs by averaging the SFR in the simulation volume over a 500 Myr period. Surface densities were calculated from volume densities by assuming a disc of thickness of 1kpc.

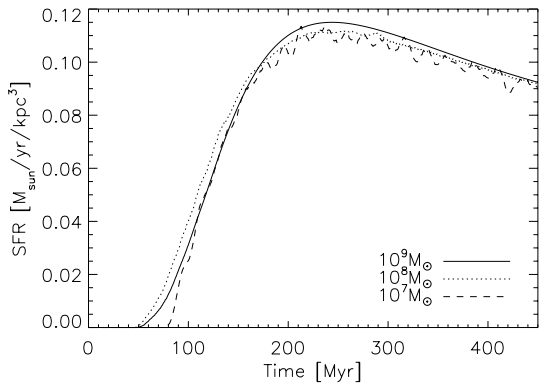

Figure 7. SFR as a function of time for one-zone models with three different mass resolutions. The SFR remains almost unchanged over two orders of magnitude in mass resolution. The coarsest mass resolution of $10^9\,M_\odot$ corresponds to the entire one-zone system being represented with a single particle with all clouds interactions modelled with the coagulation equations.

resolved particle (Fig. 7, line with mass resolution of $10^9\,M_\odot$) where all of the physics is followed by integrating the sub-grid equations in a single particle and simulations with a hundred particles that are followed explicitly.

As stated in previous sections, the behaviour of a one-zone model is virtually independent of its initial temperature and the fraction of the gas that starts off in the cold phase. This behaviour is demonstrated in Fig. 8. A one-zone volume with total initial density of $n_0 = 2\,cm^{-3}$ was evolved with a variety of different initial values for the initial temperature and initial fraction of the mass in the hot phase. We observe that regardless of the initial choices for these two quantities the system quickly settles down to its equilibrium state. This process occurs through the opposing actions of thermal conduction and SN feedback.

Figs 9 and 10 show the behaviour of the large-scale properties of two different one-zone volumes as a function of time. The only difference in the initial conditions of the two one-zone volumes is their initial density. Fig. 9 shows the evolution of a one-zone volume with a total density of 2 atoms per cm^3; Fig. 10 shows exactly the same plots for a density of 16 atoms per cm^3. The initial temperature

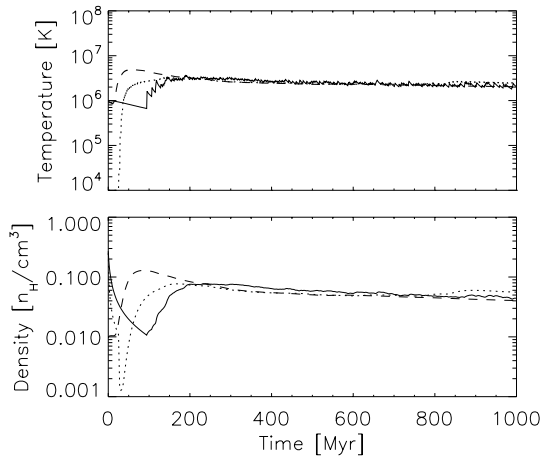

Figure 8. Temperature and density of the ambient phase of a one-zone model for a variety of different choices of initial temperature and density. The total gas density, ambient gas plus clouds, is always $2\,cm^{-3}$. The interplay of SN feedback and radiative cooling quickly brings the system into an equilibrium independent of the initial value.

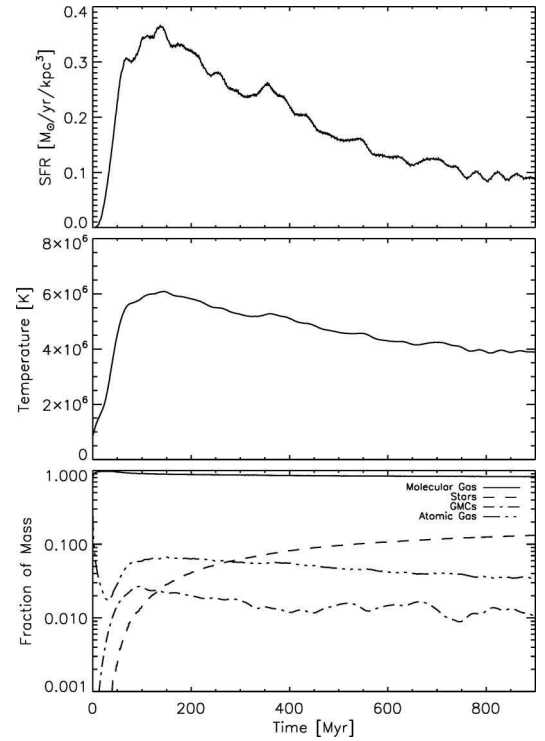

Figure 9. The large-scale properties of a one-zone model with initial density $n_0 = 2\,cm^{-3}$. The physical parameters used in this model are the same as the base model as discussed in Section 4.1.2

of the hot phase in both simulations is 10^6 K. In both cases the SFR follows the same general shape. There is a small period of time at the beginning of the simulation where small clouds are coagulating and there is no star formation. When GMCs are formed there is a large burst of star formation that is quickly quenched by feedback SN and thermal conduction in SN bubbles. The temperature of the diffuse phase is regulated by a combination of SN feedback (acting to increase the temperature) and radiative cooling. Due to the fact that we do not allow mass to leave the one-zone volume and also assume instantaneous recycling, the temperature profile very closely

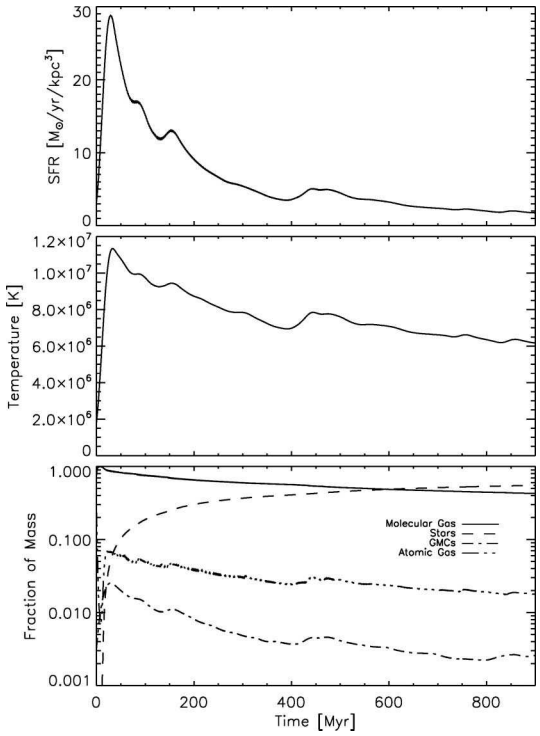

Figure 10. The same as Fig. 9 except with an initial gas density of $n_0 = 16$ cm^{-3}.

matches that of the SFR. It is noted that in the one-zone simulation with the largest density, the temperature of the ambient phase is held at a higher temperature by the action of SNe. The fraction of the gas in the molecular phase is lower in the high-density simulation due to the increased amount of evaporation by thermal conduction in the high-temperature ambient phase. In the following sections, the star formation and feedback prescriptions are tested in a more realistic situation.

5 RESULTS

As a more physically interesting test of the star formation model, we have conducted simulations of various isolated model galaxies. In this section, we introduce the details of the two different types of simulation performed and present the properties of the stellar disc and associated ISM in each case.

5.1 Quiescent disc

One of the fundamental properties that a star formation prescription must be able to reproduce is that in MW-like conditions, the resulting behaviour should be similar to that in the MW. In this section, we discuss the properties of galaxy simulations set up to approximate the conditions in the MW 's quiescent disc.

5.1.1 Simulation details

We set up a simplified model of a MW-type galaxy using initial conditions from GALACTICS (Kuijken & Dubinski 1995). GalactICS generates near-equilibrium distributions of collisionless particles consisting of a disc, bulge and halo. These models consist of a spherical bulge component; an approximately exponential disc, which is rotationally supported in the x–y plane and supported by random motion in the z-direction; and an approximately spherical halo.

Table 1. Initial particle masses in three different realizations of the model GALACTICS galaxy that are used throughout this paper. The disc and bulge consist entirely of baryons; the halo additionally contains DM. All masses are in units of $M_\odot$. Baryons are added to the DM halo by converting a random 1 per cent of the halo DM particles into gas. The DM particle mass in the halo is therefore the same as the gas particle mass.

Resolution ($M_\odot$)	Disc	Bulge	Halo
Low	6.6×10^6	5.84×10^6	5.6×10^6
Base	8.3×10^5	7.5×10^5	7.1×10^5
High	1.0×10^5	9.2×10^4	1.0×10^5

We add baryonic material to this distribution by converting the disc and bulge in their entirety into SPH particles at a temperature of 10^4 K. One per cent of the material in the halo is converted to baryons with a temperature of 10^6 K. The addition of baryonic material puts the system well out of equilibrium so each simulation is run adiabatically for 50 Myr to allow for the galaxy to relax closer to its equilibrium state before the additional physics is allowed to operate. The total mass in the disc, bulge and halo are 1×10^{10}, 0.43×10^{10} and 1.1×10^{11} $M_\odot$, respectively. The mass resolution of particles in each of the three realizations of this galaxy is summarized in Table 1. These masses were chosen such that the gaseous particles in each of the three components have approximately the same mass and the DM halo particles have masses as close as possible to the gas particle mass. The gravitational softening for the disc particles (i.e. gas, sticky and star) is set to 0.1, 0.05 and 0.02 kpc in simulations GAL_LORES, GAL_BASE and GAL_HIRES, respectively. The DM particles have softening lengths 10 times larger than that of the disc particles.

The GALACTICS simulations provide a test of the code in a situation somewhat similar to a quiescent MW disc. As discussed in Section 3, all simulations were performed with the entropy conserving SPH code GADGET2 (Springel 2005), with all of the physics discussed in Section 3 implemented as additional modules. Table 2 contains a brief summary of the different simulations. Typical time-step size in one of the base simulations is $\sim 10^4$ yr, although this figure is smaller at early times when bursts of SNe heat gas very strongly.

5.1.2 The base simulations

In this section we will discuss simulations run with the base set of physical parameters (Section 4.1.2). Most simulations were run at the base mass resolution as defined in Table 1.

The large-scale behaviour of the model galaxy is as follows: Immediately after switching on the additional star formation physics the dense, thermally unstable gas in the disc and bulge collapses into cold clouds, which quickly cause a large burst of star formation. After approximately 500 Myr the galaxy settles down into a quiescent state with an SFR of approximately 1 $M_\odot$ yr^{-1}. The SFR gradually decreases as the cold gas in the galaxy is consumed by stars.

It is known that in the MW, most areas of active star formation are concentrated in the galactic spiral arms (e.g. Engargiola et al. 2003). Fig. 11 shows that our simulations reproduce this behaviour. In the sticky particle model, this behaviour occurs naturally as the converging gas flows in galactic spiral arms lead to an increased merger rate and, therefore, to the presence of more star-forming clouds. Face

Table 2. Brief table of simulation references and details. $N_{\rm gas}$ shows the number of gas particles in the disc, bulge and halo combined.

Name	Details	$N_{\rm gas}$
GAL_BASE	Base GalactICs model	19 330
GAL_LORES	Base model with degraded mass resolution	2450
GAL_HIRES	Base model with improved mass resolution	255 000
GAL_BASE_LOSN	E_{51} decreased by a factor of 5	19 330
GAL_BASE_HISN	E_{51} increased by a factor of 5	19 330
GAL_BASE_LOCON	Conduction efficiency decreased by a factor of 5	19 330
GAL_BASE_HICON	Conduction efficiency increased by a factor of 5	19 330
GAL_BASE_LOZ	Gas metallicity set to 0.5 solar	19 330
GAL_BASE_HIZ	Gas metallicity set to 1.5 solar	19 330
ROT_BASE	Spherical rotating collapse	15 000
ROT_LORES	Spherical rotating collapse	4000
ROT_HIRES	Spherical rotating collapse	45 000

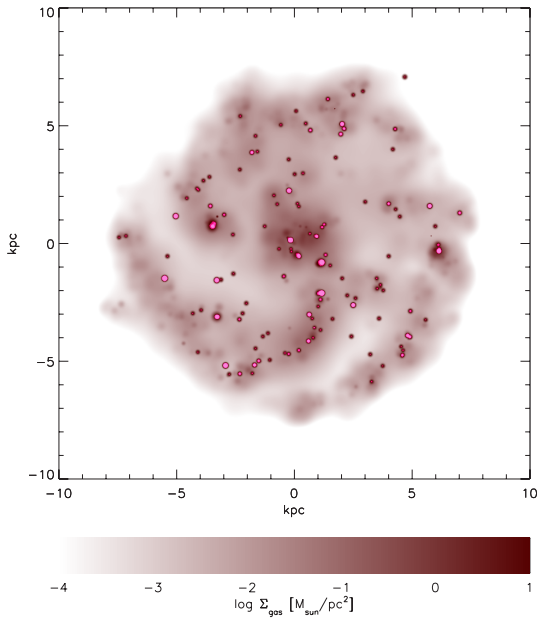

Figure 11. Demonstration of the star formation properties of the isolated galactic disc. The continuous field represents the molecular gas surface density of the simulated galactic disc, spiral structure is evident. The points represent the sites of star formation within the previous 10 Myr. Most star formation events represent the collapse of a single GMC, resulting in the formation of $10^5\,{\rm M}_\odot$ of stars. It is clear that star formation is occurring primarily in the spiral arms of the galaxy.

and edge on temperature and density plots of the standard resolution galaxy are shown in Fig. 12. The gas heated by SNeII is preferentially situated perpendicular to the plane of the disc, suggesting that the feedback scheme is preferentially heating the low-density gas and setting up strong outflows. Fig. 13 shows the behaviour of the SN-heated gas in a thin slice through the centre of the disc. Initially there is a strong burst of star formation (lower panel of Fig. 13), followed shortly by a burst of SN explosions that heat the gas around the galactic disc as hot at 10^8 K. Most of this gas is driven straight out of the halo in a direction perpendicular to the galactic disc. Later on, as the SN rate dies down, gas is heated more gently and is ejected from the galactic disc in the form of a fountain reminiscent of the galactic fountains present in the MW. This behaviour is demonstrated in Fig. 14, which shows for a random subset of particles from the gas disc the number of times they have been heated as a function of time with their height above the galactic disc. It is clear that on being strongly heated, some particles are ejected from the galactic disc and fall back down a few hundred Myr later. Others remain in dense regions and cool immediately. Some escape the disc completely in the form of a galactic wind. This behaviour was also observed in the multiphase star formation models of Scannapieco et al. (2006), suggesting that it is a more general feature of multiphase models.

Additionally our simulated galaxies are in good agreement with the observed Schmidt law, equation (15). This behaviour arises due to the self-regulation of the simulated ISM. At higher densities more molecular clouds are formed and so SFRs are higher. Runaway star formation is prevented by various forms of stellar feedback, which prevent too many clouds from forming. The slope of the Schmidt law in the simulated galaxies may be changed by altering the value of $v_{\rm stick}$. Higher values of $v_{\rm stick}$ lead to clouds coagulating more rapidly, and so low-density regions of the galactic disc undergo more star formation. The effect is less severe in the higher-density regions of the galaxy as strong feedback from large bursts of star formation can effectively regulate the amount of star formation. Conversely, a lower value of $v_{\rm stick}$ leads to a steeper Schmidt law with a lower overall SFR. This behaviour is demonstrated in Fig. 4 for the one-zone model. The value of $v_{\rm stick}$ used to reproduce the Schmidt law slope and normalization in the one-zone model also works in the simulated galaxy and the observed galaxy follows the observed Schmidt law very closely throughout its whole lifetime (Fig. 15).

The resolution independence of the star formation prescription is once again demonstrated in Fig. 16. The SFR between the highest and lowest mass resolution simulations is in remarkably good agreement. The general form followed by all simulations is that there is a strong burst of star formation at the initial time, this is rapidly quenched by SN feedback, and a self-regulating ISM is set up. The SFR slowly increases as the gas in the galactic disc is either used up or ejected in the form of winds.

Recent observations of the gas content of the MW have allowed the construction of maps of its gas surface density (Levine, Blitz & Heiles 2006). In order to compare the properties of our model to observations, another GalactICs model was generated with properties as close as possible to those of the MW. The total mass of the galactic disc was set to $5 \times 10^{10}\,{\rm M}_\odot$, and the scale radius of the exponential disc to 4.5 kpc. This simulation was evolved for 1 Gyr. The resulting gas distribution is shown in Fig. 17. Our simulations

© 2007 The Authors. Journal compilation © 2007 RAS, MNRAS **376,** 1588–1610

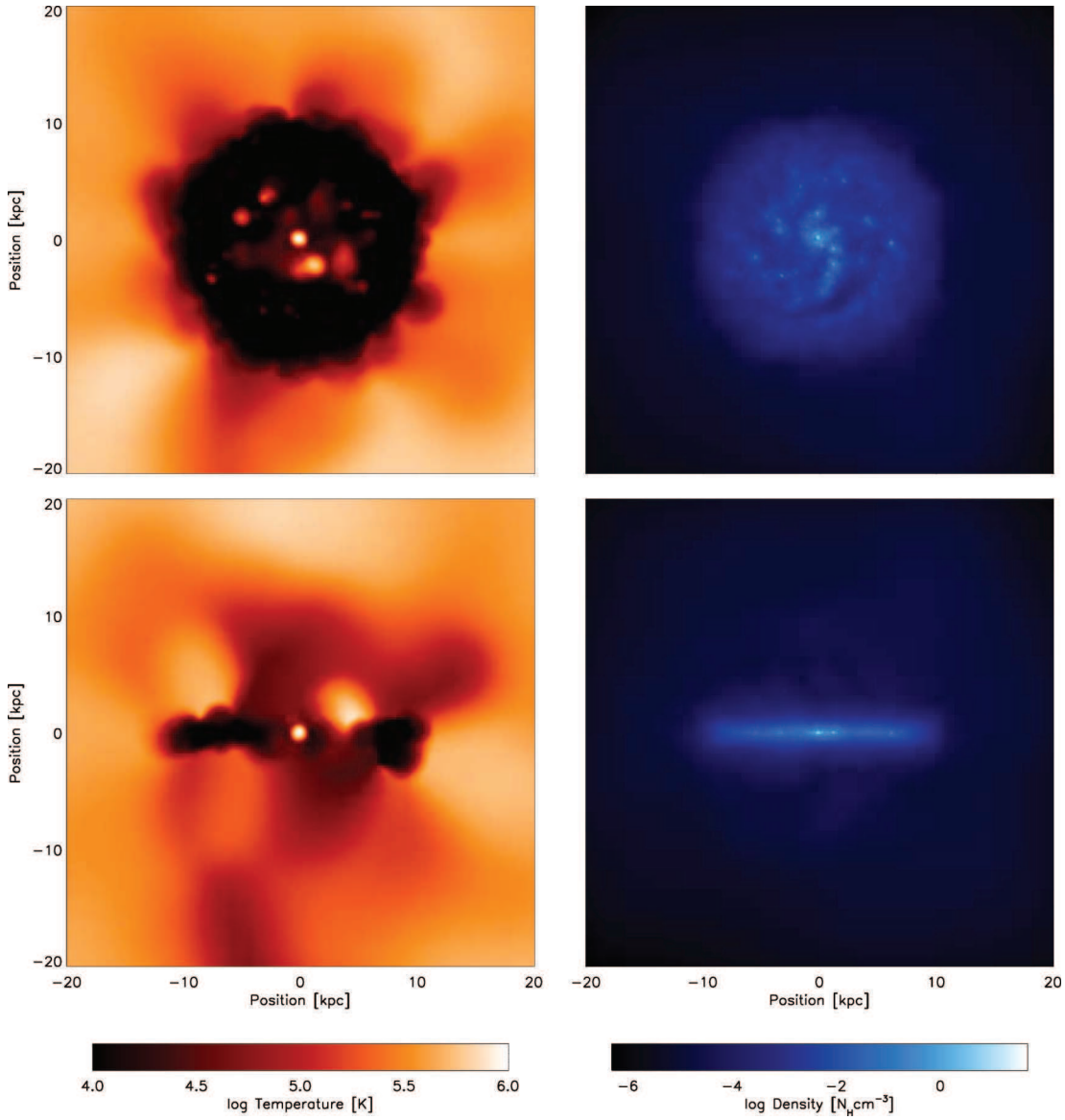

Figure 12. A thin slice of the gas temperature and density distributions after 1 Gyr in run GAL_BASE. The slice is taken directly through the centre of mass of the stellar disc. The temperature plot clearly shows regions of strongly heated gas; these are areas near to sites of active star formation, where the massive, short-lived stars are heating the ambient material via SN explosions.

are in good agreement with the observations of Levine et al. (2006).

These properties suggest that the star formation and feedback prescriptions behave well in a quiescent disc, a more robust test of how they perform in a more general situation is given by the rotating collapse simulations.

5.2 Rotating collapse

5.2.1 Simulation details

The second simulation we investigate is the collapse of a rotating spherical halo (Navarro & White 1993) with an initial $1/r$ density profile consisting of 90 per cent collisionless DM and 10 per cent baryonic material. The mass of the rotating sphere is $1 \times 10^{12}\,\mathrm{M}_{\odot}$ and its initial radius is 100 kpc. Velocities are chosen such that the sphere is initially rotating as a solid body with a spin parameter of 0.1. Once again this simulation is created at three different mass resolutions, corresponding to DM particle masses of 5.2×10^{8}, 5.8×10^{7} and $2.0 \times 10^{7}\,\mathrm{M}_{\odot}$, with corresponding gravitational softenings of 1.93, 0.96 and 0.68 kpc. The rotating collapse simulations model, in a crude way, the collapse of a protogalaxy, and allow us to investigate how the ISM model behaves when it is initially far from equilibrium and in situations with strong shocks and rapid density changes.

5.2.2 The base simulations

After 2 Gyr the density profiles of each of the three phases of matter are shown in Figs 18 and 19. The density profiles are averaged around the disc; each radial bin represents a ring centred on the centre of mass of the disc. Fig. 18 shows the radial density profiles of both the ambient and molecular gas. The three different resolution simulations once again behave in very similar ways. Fig. 19 shows

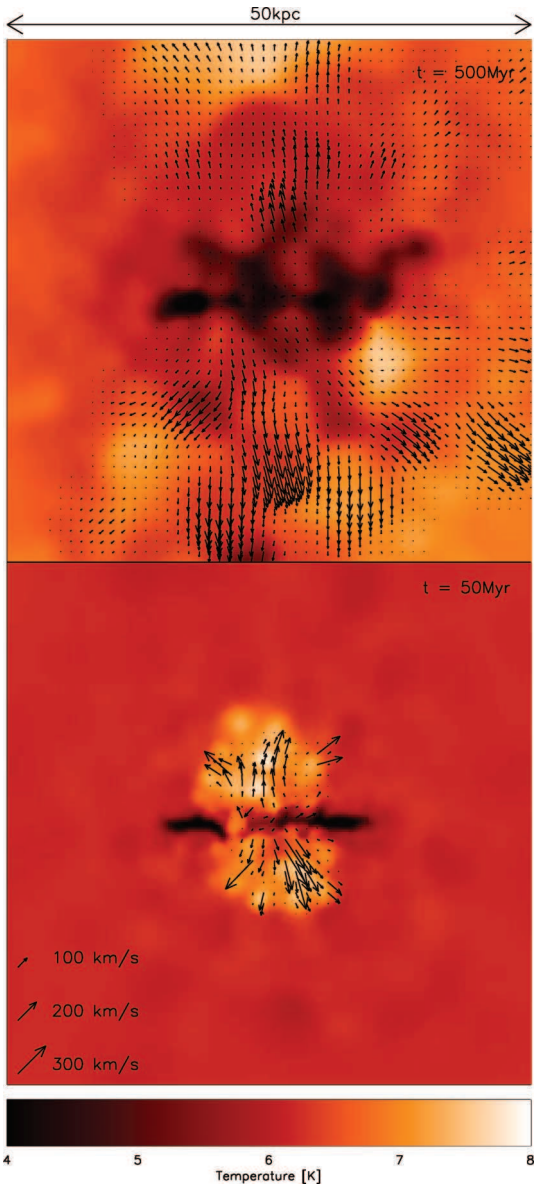

Figure 13. A thin slice of the gas temperature field through the centre of a disc galaxy simulation. The arrows represent the gas velocity field, taking into account only gas that has been heated by SNe. The generation of bipolar outflows from the galactic disc is very clear. The lower plot represents the galaxy after 50 Myr; the upper panel is the same galactic disc after 500 Myr.

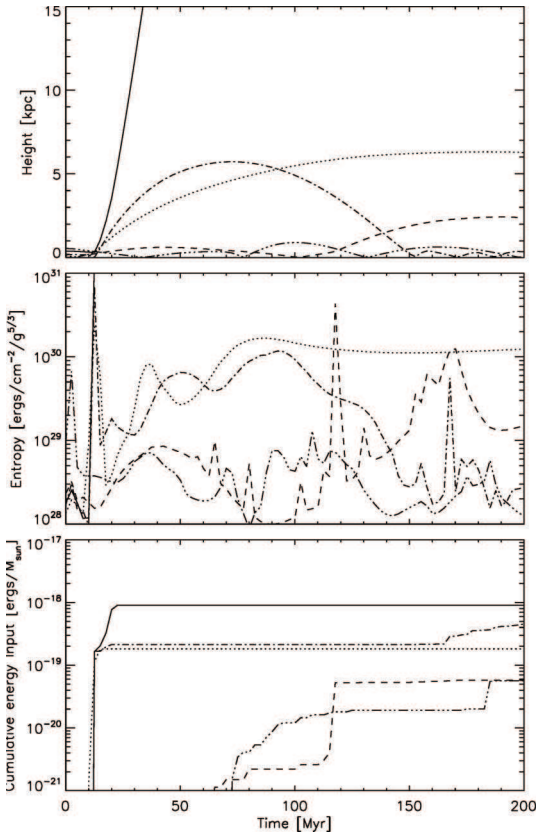

Figure 14. Relationship between the number of SN heatings and the distance from the mid-plane of the disc for a sampling of five particles from the simulated galaxy. Each different linestyle represents a different SPH particle. The top panel shows the perpendicular distance from the centre of the stellar disc, the central panel shows the entropy of each particle and the lower panel the cumulative amount of thermal energy that has been dumped into the particle. It is clear that some particles with a higher entropy are lifted away from the galactic disc where they cool and rain back down on the galactic disc within 100 Myr of being SN heated. Other particles are ejected violently from the galaxy; their density becomes very low and they evolve adiabatically.

the radial density profile of stellar mass, demonstrating that our star formation prescription gives rise to an exponential disc and a bulge component well fitted by the standard $r^{1/4}$ law.

The rotating collapse simulations are especially interesting because they start far from equilibrium and so features that arise in the final particle distribution are purely an effect of the physics in the simulation and not just set up by hand in the initial conditions. Fig. 20 shows how the molecular fraction (the ratio of the mass in molecular hydrogen to the mass in atomic hydrogen) varies as a function of distance from the centre. Observational data from M31 (Dame et al. 1993) are included as a comparison.

The evolution of the thermal properties of the halo is shown in Fig. 21. In its initial state all the gas in the halo is cold. As the halo collapses it becomes dense and is shock heated. The gas that ends

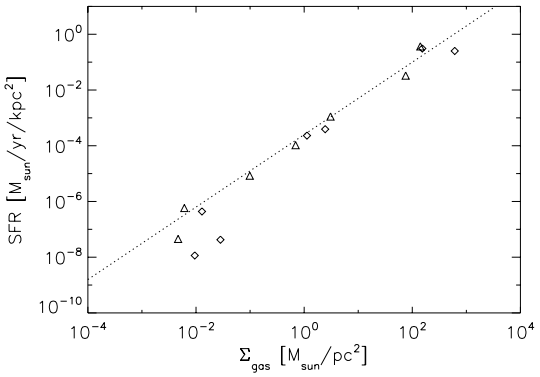

Figure 15. The density–SFR relationship for our simulated quiescent disc. The diamond shaped points represent the observed SFRs after 200 Myr, and the triangles represent the SFRs in the same disc after 1 Gyr. The dashed line is the observed Schmidt law due to Kennicutt (1998). The points on this plot were calculated by taking radial bins, then calculating the mean density and SFR in each bin over a short period. The quiescent galaxy follows the observed Schmidt law throughout its lifetime.

© 2007 The Authors. Journal compilation © 2007 RAS, MNRAS **376,** 1588–1610

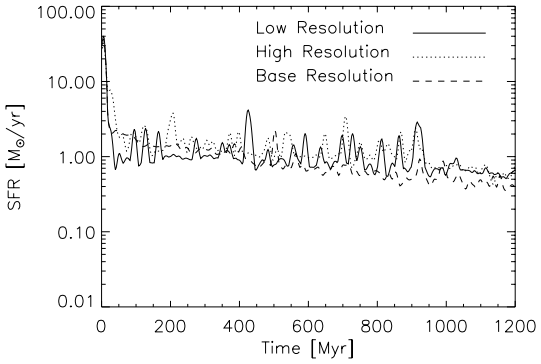

Figure 16. SFR as a function of time for isolated galaxy models with different mass resolutions. The mass resolution is 64 times better in the high-resolution disc than the low-resolution one. The three simulations plotted are GAL_LORES, GAL_BASE and GAL_HIRES. The fact that the SFR remains almost unchanged shows that numerical convergence has been achieved.

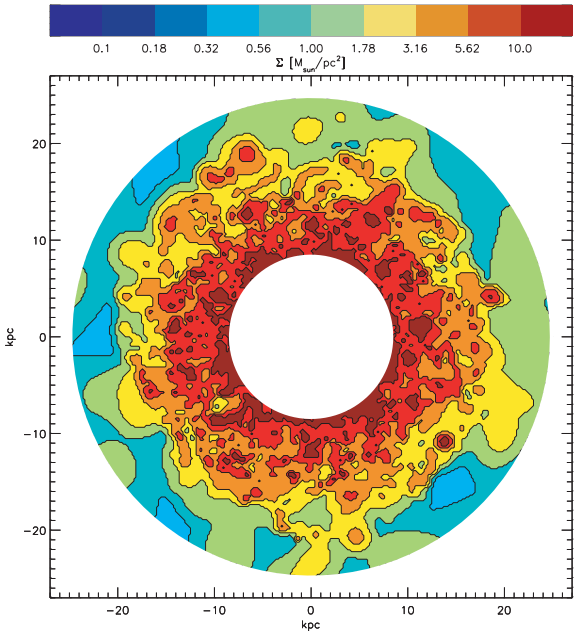

Figure 17. Plot of the distribution of gas atomic in a galactic disc after 500 Myr of evolution. Colours and plot dimensions are matched to those in Levine et al. (2006) for easy comparison to observations. The inner circle represents the radius from the centre of the galaxy to the position of the Sun. The outer radius is where the observations of Levine et al. (2006) are truncated. The simulated MW has a surface density profile in close agreement with that observed by Levine et al.

up in the disc comes to an equilibrium between radiative cooling and the heating due to SNe at approximately 10^4 K and a halo of hot, SN-heated gas at $\sim 10^6$ K is gradually formed. The addition of the molecular gas ($T \sim 100$ K, $\rho \sim 100$–$1000\,\mathrm{cm}^{-3}$) forms an ISM with four phases: shocked halo gas, SN-heated material, cold molecular clouds and warm disc gas. The first two components are hard to distinguish on the ρ –T plot.

Blitz & Rosolowsky (2006) have argued that the ratio of molecular to atomic gas in galaxies, R_{mol}, is determined by hydrostatic pressure and through observations of nearby galaxies found the following relation:

$$R_{\mathrm{mol}} = \left[\frac{P_{\mathrm{ext}}/k_{\mathrm{B}}}{(3.5 \pm 0.6) \times 10^4}\right]^{0.92\pm0.07}, \qquad (27)$$

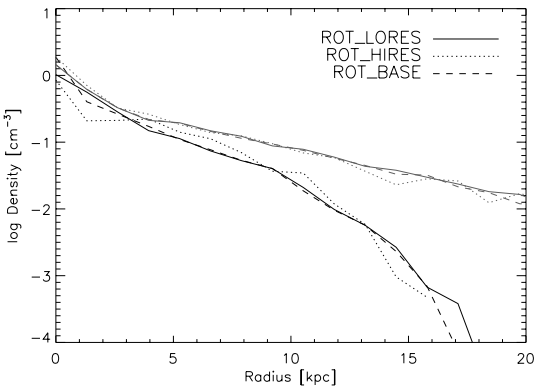

Figure 18. Density profiles for the ambient material (grey lines) and the molecular clouds (black lines). The solid lines represent the low-resolution rotating collapse simulations and the dotted lines represent the highest-resolution simulations. Agreement between the high- and low-resolution simulations is very good.

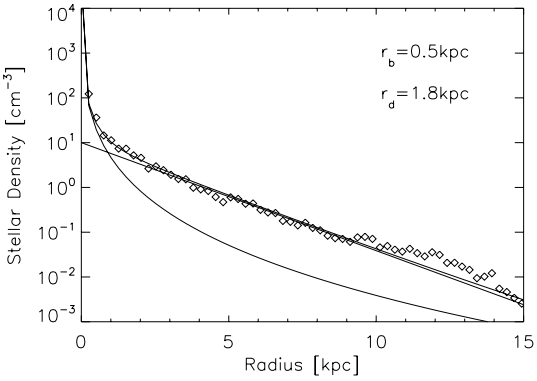

Figure 19. Stellar density profile in the base rotating collapse simulation. The solid lines represent the best-fitting exponential and a de Vaucouleurs profile. The scale radii used in the exponential and de Vacouleurs fits are r_{d} and r_{b}, respectively. It is clear that even starting from an initial condition far from equilibrium we generate a stellar disc with a surface density profile similar to that in observed galaxies.

where P_{ext} is an estimate of the mid-plane pressure, and R_{mol} is the ratio of mass in the atomic and molecular phases. Fig. 22 shows the data for the ROT_BASE simulation after 1 Gyr alongside the observed best-fitting line (equation 26). We use the SPH estimate of the pressure at $z = 0$. To calculate R_{mol} we use all matter within a vertical distance of 1 kpc from the centre of mass of the disc and bin radially. The model of the ISM clearly reproduces the observed behaviour.

5.3 Away from the base model

The determination of some of the physical parameters used in our model is somewhat uncertain. In this section we investigate the effect of varying some of the physics included in the models. Large uncertainties are present in the determination of some of the parameters including E_{51}, the thermal conduction efficiency, and the physics we include in our treatment of SN explosions. In addition our simulations do not contain a detailed treatment of metals. We demonstrate the effects of changing each of these parameters on the large-scale properties of simulated quiescent discs.

The value of E_{51} may differ greatly from unity, for example, due to radiative cooling of the SN remnant. We investigate the effect of

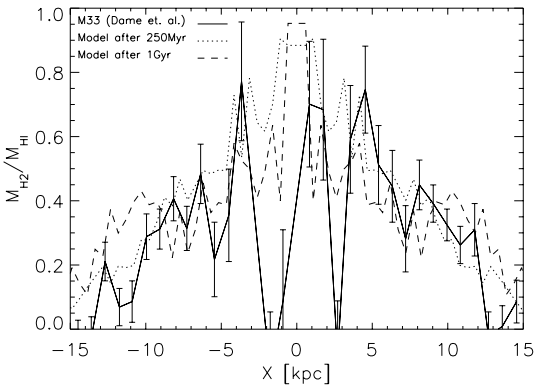

Figure 20. Fraction of gas in the molecular phase as a function of distance from the centre of the galactic disc for the rotating collapse model at two different times. The solid line represents the same data as plotted from M31 (Dame et al. 1993), with the x-axis representing position along the major axis of the galaxy. The simulated galactic disc is in good agreement with observation.

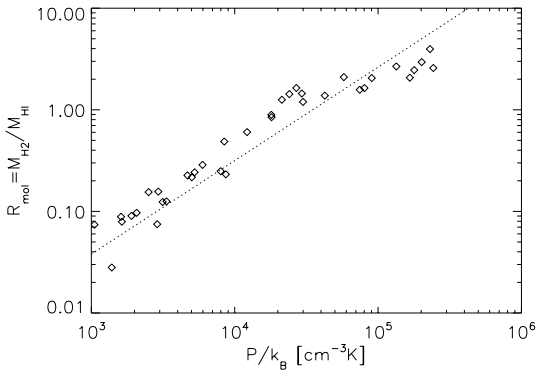

Figure 22. The relation between the pressure in the mid-plane of the galactic disc and the ratio of gas in the molecular phase to the atomic phase, $R_{\rm mol}$. The dotted line represents the observational result (equation 26) due to Blitz & Rosolowsky (2006). The simulated galaxy is in good agreement with observation.

moving E_{51} away from unity and also look at changing the physics included in our analytic model for blast wave evolution, first by extending the simple Sedov solution with the fitting formula due to Tang & Wang (2005) and secondly by investigating the effects of preventing radiative cooling in SN remnants.

Altering the value of E_{51} has, as expected, two main effects. First, an increased SN efficiency can eject gas from the galactic disc more efficiently and quenches star formation very quickly. Secondly, the gas disc in simulations with higher SN efficiency is found to be less centrally concentrated; the reverse is also true in simulations with

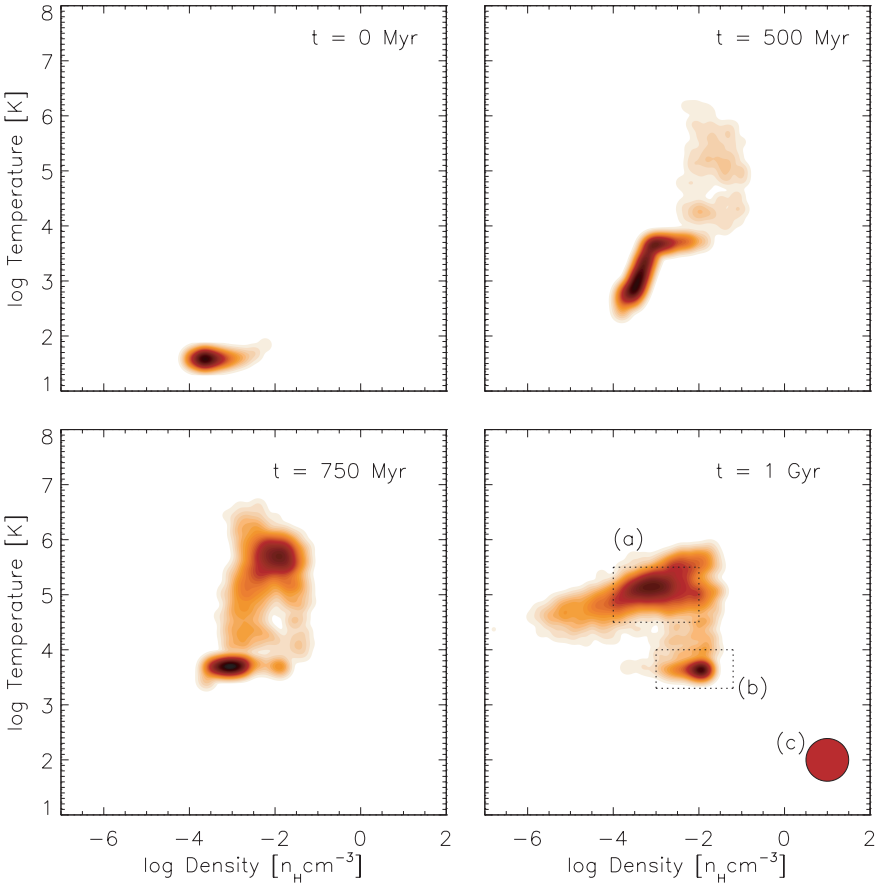

Figure 21. Density–temperature relation for a rotating collapse simulation showing the creation of three distinct components. In the final time plot region (a) contains gas in the halo of the galaxy. Region (b) is gas in the disc of the galaxy, which reaches an equilibrium temperature of $\sim 10^4$ K and region (c) represents the approximate position of the molecular clouds, at an assumed temperature of 100 K. The gas in the halo consists of both gas that failed to cool on to the disc and gas that was originally in the disc but has been heated by SNe. Approximately 45 per cent of the mass is in the two hot phases, 40 per cent in the disc and 15 per cent in the cold molecular clouds.

© 2007 The Authors. Journal compilation © 2007 RAS, MNRAS **376,** 1588–1610

a low SN efficiency. This is a result of SN feedback ejecting gas from the galactic disc more efficiently in the runs with a high value of E_{51}. We find that the fiducial value of $E_{51} = 1.0$ provides a good match with the observed properties of disc galaxies.

More accurate modelling of the evolution of SN blast waves (by using the Tang & Wang 2005 fit to the blast wave evolution) does not significantly change the properties of the galaxy. Assuming that a typical SN remnant expands for approximately $\sim$0.3 Myr before being dispersed, that the mean ambient temperature of the ISM is 10^6 K and the mean density is 10^{-2} atoms per cm^3 then the difference in the blast wave radius between the pure Sedov solution (10) and the modified fitting formula due to Tang & Wang (2005) (equation 11) is never more than 20 per cent. This is demonstrated in Fig. 2, which shows a pure Sedov blast wave compared with the simulated result from an SPH simulation of a blast wave in a hot (10^6 K) medium.

The net result of having larger blast waves is that the porosity of the ISM increases at a greater rate and the delay between an SN explosion occurring and its thermal energy being injected into the ambient medium is decreased.

Finally we can switch off the radiative cooling in SN remnants. The effects here are much more dramatic. In the dense galactic disc, an SN remnant can typically radiate away over 90 per cent of its thermal energy before being disrupted. Switching off radiative cooling in SN remnants, therefore, has a very severe effect in our galaxy simulations, and leads to the almost immediate suppression of star formation and much of the material in the galactic disc is ejected from the galaxy. This demonstrates that radiative losses from SN remnants are of crucial importance in our models.

Our simulation code does not contain a detailed description of mass feedback from SNe. Therefore, we need to verify that the expected evolution in metallicity over the time-scale of the simulation will not substantially affect the properties of the galactic disc.

Following Harfst et al. (2006) we use a simple analytic model to estimate the change in metallicity over the time-scale of a typical simulation and then run simulations with metallicities bracketing this range. By assuming that stars form at a constant rate of $1\,\mathrm{M}_\odot\,\mathrm{yr}^{-1}$, that there is one type 2 SN event per 125 $\mathrm{M}_\odot$ of stars formed, and using metal yields due to Woosley & Weaver (1995) we estimate that over the 1 Gyr time-span of one of the quiescent disc simulations the average metallicity of the galaxy should not change by more than $0.04\,\mathrm{Z}_\odot$.

The base simulations have a metallicity of $1.0\,\mathrm{Z}_\odot$, two additional simulations were run with metallicities of 0.5 and $1.5\,\mathrm{Z}_\odot$, far outside the metallicity evolution range expected in our quiescent discs. The total amount of stars after 1 Gyr in the high-metallicity run is 5 per cent higher than that in the base run. The low-metallicity run contains approximately 5 per cent less stars than the base run. This trend arises because the radiative cooling rate of the ambient phase is related to the ambient gas metallicity. All the properties of the three simulated discs agree to within 10 per cent with the properties of the base simulations. The reason for the surprisingly small dependence of the galaxy properties on the metallicity of the gas is that in the quiescent disc the gas is maintained at a temperature of $\sim 10^4$ K. At this temperature the radiative cooling function does not change very much with metallicity. We do, however, note that a full treatment of the metal enrichment of the gas is necessary in performing fully cosmological simulations since here the metallicity of the gas may significantly affect the way in which it collapses (e.g. Scannapieco et al. 2005). In these simulations we have additionally neglected the change in stellar lifetime with metallicity (see e.g. Raiteri, Villata & Navarro 1996). Since we are simulating a quiescent disc, it is not expected that changes to the lifetimes of massive stars will have a large effect on the properties of the galactic disc.

However, as noted by Harfst et al. (2006) a detailed prescription for the yields from SNe is necessary if we want to simulate the early evolution of a galaxy.

One of the most poorly constrained parameters is the efficiency of evaporation of molecular clouds through thermal conduction. Magnetic fields and turbulence may affect the amount of thermal conduction by a large amount (MO77). We ran quiescent disc simulations with the efficiency of thermal conduction moved by a factor of 5 in each direction (GAL_BASE_LOCON; GAL_BASE_HICON). More efficient thermal conduction leads to a lower density of molecular clouds in the galactic disc, as well as making the cloud mass function more shallow. The SFRs are affected by a similar amount; in the simulations with a high thermal conduction rate the SFR is depressed by an order of magnitude. As discussed in Section 5.2 the base value for the thermal conduction efficiency reproduces many of the observed properties of the MW.

6 CONCLUSIONS

Motivated by the fact that we cannot reasonably resolve the Jeans scale for molecular clouds in galaxy simulations we have introduced a new star formation and feedback prescription. We model the ambient phase of the ISM using a hydrodynamic simulation code and the unresolved molecular gas using a sticky particle prescription. Our model leads to a tightly self-regulating multiphase ISM. The multiphase nature of our star formation prescription avoids a lot of the problems of overcooling that were present in the first generation of star formation models. With the exception of the parameter that controls the molecular cloud coagulation time-scale, v_{stick}, all the parameters in our model can be tightly constrained by observation, leaving the cloud coagulation time-scale as a free parameter that we can adjust to match the observed properties of galaxies. Where possible our model of the ISM has been formulated in such a way that the results of a simulation should be independent of mass resolution. We demonstrated that the large-scale properties of our simulations were unchanged over a two orders of magnitude shift in mass resolution.

We have applied the sticky particle star formation model to three different types of simulation: a simple one-zone model, the rotating collapse of a gas and DM sphere and a model of a quiescent galactic disc. After using the one-zone simulation to set the value of the parameters that cannot be determined observationally, the sticky particle model can be applied to the other simulations without any parameter changes.

The simulations of a quiescent disc galaxy reproduce the observed Schmidt law with a slope of 1.4 due to the opposing effects of cloud coagulation and feedback effects. The galaxy also developed a natural three-component ISM. Finally, we observe SN-heated gas in the galaxy being ejected from the disc either in the form of a galactic fountain, or, when the SFR (and associated SN rate) is sufficient, in the form of strong bipolar outflows. Both of these results arise as a natural consequence of the physics included in our star formation prescription.

Simulations of the collapse of a rotating sphere of DM and gas reproduced many of the observed properties of galactic discs beginning from an initial condition well out of equilibrium. In particular we observe a stellar disc with distinct bulge and disc components, well fitted by the standard exponential and de Vacouleurs density profiles. The fraction of molecular gas in the disc as a function of radius is reproduced, and agrees well with recent observations of

nearby galaxies. The observed relation between the disc mid-plane pressure and the fraction of molecular clouds is also reproduced. We also observe SFRs comparable to those in disc galaxies and note that our model reproduces the formation of stars in the spiral arms of the galaxy.

Our preferred values for most of the parameters are discussed in Section 4, and are usually constrained by observation. We varied the values of parameters that are only weakly constrained by observation and found that in all cases our default values produced reasonable results. Including different physical descriptions of the evolution of SN blast waves makes only a modest difference to our results. Finally, we note that in the quiescent disc simulation our results depend relatively weakly on metallicity, although this will not be the case in fully cosmological simulations, for which a full treatment of metal enrichment via SN feedback is necessary.

A natural continuation of this work is to extend our investigations to higher redshift through the use of fully cosmological simulations, and to explore the behaviour of the ISM in colliding galaxies. This work is currently being pursued.

ACKNOWLEDGMENTS

CMB and TT thank PPARC for the award of a research studentship, and an Advanced Fellowship, respectively. TO acknowledges financial support from the Japan Society for the Promotion of Science for Young Scientists (1089). We are grateful to Volker Springel for providing us with the GADGET2 code, to Joop Schaye, Claudio Dalla Vecchia, and Rob Wiersma for providing us with tabulated radiative cooling and heating rates and to Peter Thomas, Pierluigi Monaco, Gustavo Yepes and Richard Bower for useful discussions. Finally, we thank the anonymous referee for their careful reading of this manuscript, which has substantially improved the logical flow and clarity of this paper. All simulations were performed on the Cosmology Machine at the Institute for Computational Cosmology in the University of Durham.

REFERENCES

Abel T., Bryan G. L., Norman M. L., 2000, ApJ, 540, 39
Ballesteros-Paredes J., Vázquez-Semadeni E., Scalo J., 1999, ApJ, 515, 286
Begelman M. C., McKee C. F., 1990, ApJ, 358, 375
Benson A. J., Kamionkowski M., Hassani S. H., 2005, MNRAS, 357, 847
Binney J., Merrifield M., 1998, Galactic Astronomy, Princeton Univ. Press, Princeton, NJ
Blitz L., Shu F. H., 1980, ApJ, 238, 148
Blitz L., Thaddeus P., 1980, ApJ, 241, 676
Blitz L., Rosolowsky E., 2004, ApJ, 612, L29
Blitz L., Rosolowsky E., 2006, ApJ, 650, 933
Blitz L., Fukui Y., Kawamura A., Leroy A., Mizuno N., Rosolowsky E., 2006, in Reipurth B., Jewitt D., Keil K., eds, Protostars and Planets V. Univ. Arizona Press, Tucson, p. 81
Bonnell I. A., Bate M. R., Clarke C. J., Pringle J. E., 1997, MNRAS, 285, 201
Bonnell I. A., Dobbs C. L., Robitaille T. P., Pringle J. E., 2006, MNRAS, 365, 37
Burkert A., 2006, Comptes Rendus Phys., 7, 433
Cen R., Ostriker J. P., 1992, ApJ, 399, 113
Chevalier R. A., 1975, ApJ, 198, 355
Cowie L. L., McKee C. F., 1977, ApJ, 211, 315
Croft R. A. C., Davé R., Hernquist L., Katz N., 2000, ApJ, 534, 123
Dame T. M., Koper E., Israel F., Thaddeus P., 1993, ApJ, 418, 730
Dekel A., Silk J., 1986, ApJ, 303, 39
Dobbs C. L., Bonnell I. A., 2006, MNRAS, 367, 873
Efstathiou G., 2000, MNRAS, 317, 697
Elmegreen B. G., 1983, MNRAS, 203, 1011
Elmegreen B. G., 1996, in Blitz L., Teuben P., eds, IAU Symp. Vol. 169, Unsolved Problems of the Milky Way. Kluwer, Dordrecht, p. 551
Elmegreen B. G., 2000, ApJ, 530, 277
Engargiola G. L., Plambeck Rl L., Rosolowsky E., Blitz L., 2003, ApJS, 149, 343
Ferland G. J., Korista K. T., Verner D. A., Ferguson J. W., Kingdon J. B., Verner E. M., 1998, PASP, 110, 761
Field G. B., Goldsmith D. W., Habing H. J., 1969, ApJ, 155, 149
Fukui Y., Mizuno N., Yamaguchi R., Mizuno A., Onishi T., 2001, PASJ, 53, 41
Gingold R. A., Monaghan J. J., 1977, MNRAS, 181, 375
Gomez M., Jones B. F., Hartmann L., Kenyon S. J., Stauffer J. R., Hewett R., Reid I. N., 1992, AJ, 104, 762
Haardt F., Madau P., 1996, ApJ, 551, 852
Haardt F., Madau P., 2001, in Neumann D. M., Van J. T. T., eds, Clusters of Galaxies and the High Redshift Universe Observed in X-rays. EDP Sciences, Les Ulis, p. 64
Harfst S., Theis C., Hensler G., 2006, A&A, 449, 509
Heyer M. H., Carpenter J. M., Snell R. L., 2001, ApJ, 461, 20
Higdon J. C., Lingenfelter R. E., Ramaty R., 1998, ApJ, 509, L33
Hultman J., Pharasyn A., 1999, AAP, 347, 769
Jenkins A., Binney J., 1994, MNRAS, 270, 703
Jog C. J., Ostriker J. P., 1988, ApJ, 328, 404
Katz N., 1992, ApJ, 391, 502
Katz N., Weinberg D. H., Hernquist L., 1996, ApJS, 105, 19
Kawata D., Gibson B. K., 2003, MNRAS, 340, 908
Kay S. T., Pearce F. R., Frenk C. S., Jenkins A. R., 2002, MNRAS, 330, 113
Kennicutt R. C., 1989, ApJ, 344, 685
Kennicutt R. C., 1998, ApJ, 498, 541
Klamer I. J., Ekers R. D., Sadler E. M., Hunstead R. W., 2004, ApJ, 612, L97
Koyama H., Inutsuka S. I., 2000, ApJ, 532, 980
Frumholz M. R., McKee C. F., 2005, ApJ, 630, 250
Kuijken K., Dubinski J., 1995, MNRAS, 277, 1341
Kwan J., Valdes F., 1983, ApJ, 271, 604
Lada C. J., Lada E. A., 2003, ARA&A, 41, 57
Larson R. B., 1978, J. Comput. Phys., 27, 397
Lee H. B., Nelson L. A., 1988, ApJ, 334, 688
Levine E. S., Blitz L., Heiles C., 2006, Sci, 312, 1773
Levinson F. H., Roberts W. W., Jr, 1981, ApJ, 245, 465
Lin D. N. C., Pringle J. E., 1976, in Egleton P., Mitton S., Whelan J., eds, Proc. IAU Symp. 73, The Structure of and Evolution of Close Binary Systems, Reidel, Dordrecht, p. 183
Lucy L. B., 1977, AJ, 82, 1013
Mac Low M. M., Klessen R. S., 2004, Rev. Mod. Phys., 76, 125
Marri S., White S. D. M., 2003, MNRAS, 345, 561
Matzner C. D., 2002, ApJ, 566, 302
McKee C. F., 1977, ApJ, 215, 213
McKee C. F., Ostriker J. P., 1977, ApJ, 218, 148 (MO77)
Miller G. E., Scalo J. M., 1978, PASP, 90, 506
Monaco P., 2004, MNRAS, 352, 181
Monaghan J. J., 1992, ARA&A, 30, 543
Navarro J. F., Benz W., 1991, ApJ, 380, 320
Navarro J. F., White S. D. M., 1993, MNRAS, 265, 271
Okamoto T., Eke V. R., Frenk C. S., Jenkins A., 205, MNRAS, 363, 1299
Oort J. H., 1954, Bull. Astron. Inst. Netherlands, 12, 177
Padoan P., Nordlund A. A., 2002, ApJ, 576, 870
Padovani P., Matteucci F., 1993, ApJ, 416, 26
Pearce F. R. et al., 1999, ApJ, 521, 99
Pearce F. R., Jenkins A., Frenk C. S., White S. D. M., Thomas P. A., Couchman H. M. P., Peacock J. A., Efstathiou G., 2001, MNRAS, 326, 649
Pringle J. E., Allen R. J., Lubow S. H., 2001, MNRAS, 327, 663
Raiteri C. M., Villata M., Navarro J. F., 1996, AAP, 315, 105
Rees M. J., Ostriker J. P., 1977, MNRAS, 179, 541
Ritchie B. W., Thomas P. A., 2001, MNRAS, 323, 743
Roberts M. S., 1957, PASP, 69, 59

Rosolowsky E., Blitz L., 2004, Ap&SS, 289, 265
Safier P. N., McKee C. F., Stahler S. W., 1997, ApJ, 485, 660
Salpeter E. E., 1955, ApJ, 121, 161
Saslaw W. C., 1985, Gravitational Physics of Stellar and Galactic Systems. Cambridge Univ. Press, Cambridge
Scannapieco C., Tissera P. B., White S. D. M., Springel V., 2006, MNRAS, 371, 1125
Scannapieco C., Tissera P. B., White S. D. M., Springel V., 2005, MNRAS, 364, 552
Schaye J., 2004, ApJ, 609, 667
Schmidt M., 1955, ApJ, 129, 243
Sedov L. I., 1959, Similarity and Dimensional Methods in Mechanics. Academic Press, New York
Semelin B., Combes F., 2002, A&A, 388, 826
Smoluchowski M., 1916, Physik Zeit., 17, 557
Solomon P. M., Rivolo A. R., Barrett J., Yahil A., 1987, ApJ, 319, 730
Springel V., Yoshida N., White S. D. M., 2001, New Astron., 6, 79
Springel V., Hernquist L., 2003, MNRAS, 339, 289
Springel V., 2005, MNRAS, 364, 1105
Springel V. et al., 2005, Nat, 435, 629
Steinmetz M.Muller E., 1994, A&A, 281, 97
Stinson G., Seth A., Katz N.Wadsley J., Governato F., Quinn T., 2006, MNRAS, 373, 1074
Sutherland R. S., Dopita M. A., 1994, ApJS, 88, 253
Tang S., Wang Q. S., 2005, ApJ, 628, 205
Theuns T., Leonard A., Efstathiou G., Pearce F. R., Thomas P. A., 1998, MNRAS, 301, 478
Thornton K., Gaudlitz M., Janka H. T., Steinmetz M., 1998, ApJ, 500, 95
Wada K., Meurer G., Norman C. A., 2002, ApJ, 577, 197
Weil M. L., Eke V. R., Efstathiou G., 1998, MNRAS, 300, 773
White S. D. M., Rees M. J., 1978, MNRAS, 183, 341
Williams J. P., McKee C. F., 1997, ApJ, 476, 166
Wilson C. D., Scoville N., 1990, ApJ, 363, 9435
Wolfire M. G., Hollenbach D., McKee C. F., Tielens A. G. G. M., Bakes E. L. O., 1995, ApJ, 443, 152
Woosley S. E., Weaver T. A., 1995, ApJS, 101, 181
Yepes G., Kates R., Khokhlov A., Klypin A., 1997, MNRAS, 284, 235
Young J. S., Scoville N. Z., 1991, ARA&A, 29, 581

APPENDIX A: LIST OF SYMBOLS

α_c: slope of the molecular cloud mass–radius relation. Equation (2)
c_h: sound speed of the ambient gas phase
$\epsilon_\star$: fraction of a GMC converted to stars in a collapse.
η: fraction of cloud velocity lost to 'cooling' collision
E_{51}: energy ejected per SNeII in units of 10^{51} erg
E_b: total energy in an SN blast wave
E_m: total kinetic energy in molecular clouds of mass m in a given volume
f_{cl}: filling factor of cold clouds $f_m(\sigma_1, \sigma_2)$: fraction of collisions between clouds with velocity dispersions σ_1 and σ_2 that lead to mergers $K(m, m')$: the kernel for aggregation of clouds of masses m and $m\prime$. Equation (3)
λ: constant of proportionality relating cloud mass and destruction rate by thermal conduction. Equation (22)
Λ_N: normalized radiative cooling rate
Λ_{net}: net radiative cooling rate (erg cm^{-3} s^{-1})
M_c: mass of a molecular cloud
M_{char}: characteristic mass resolution of a simulation
M_{ref}: reference cold cloud mass. Equation (2)
$M_{\star,min}$: minimum allowed star mass
$M_{\star,max}$: maximum allowed star mass
n_b: density internal to an SN remnant in atoms cm $^{-3}$
n_c: density of a molecular cloud in atoms cm $^{-3}$
n_h: density of the ambient medium in atoms cm $^{-3}$
N_{SF}: the slope of the schmidt law. Equation (8)
$n(m, t)$: the number of clouds with masses between m and $m + dm$
$N(m, t)$: the number density of clouds with masses between m and $m + dm$
ϕ: efficiency of destruction of cold clouds by thermal conduction
Q: porosity of the ISM. Section 3.4.2
r_c: radius of a molecular cloud
r_{ref}: reference cold cloud radius. Equation (2)
r_b: the radius of a spherical blast wave
ρ_c: mean density of molecular clouds contained in a volume
ρ_h: mean density of ambient gas contained in a volume
ρ_{th}: density at which ambient gas becomes thermally unstable
ρ_{SFR}: volume density of star formation
T_b: mean temperature inside an SN remnant
T_c: internal temperature of cold clouds
T_h: temperature of the ambient gas phase
u_b: thermal energy per unit mass of SN remnants
u_c: thermal energy per unit mass of the cold clouds
u_h: thermal energy per unit mass of the ambient phase
Σ: cross-section for collision between clouds. Equation (4)
Σ_{cond}: efficiency of thermal conduction. Equation (18)
v_{app}: relative approach velocity of two molecular clouds
v_{stick}: maximum relative velocity for cloud merger
x: slope of the stellar IMF

APPENDIX B: ENERGY TRANSFER THROUGH COAGULATION

Our formalism to treat the evolution of the mass function of clouds internal to each of the 'multiple cloud' particles will start from the Smoluchowski equation of kinetic aggregation (Smoluchowski 1916):

$$\frac{\partial n}{\partial t} = \tfrac{1}{2V}\int_0^\infty n(m', t)n(m - m', t)K(m', m - m')\,\mathrm{d}m' - \frac{1}{V}n(m, t)\int_0^\infty n(m', t)K(m, m')\,\mathrm{d}m', \tag{B1}$$

where $n(m, t)$ represents the number of clouds with masses between m and $m + dm$ contained within a volume, V and $K(m, m')$ represents the kernel for aggregation of clouds with masses m and m', as defined by equation (3).

The fraction of collisions between clouds of masses m_1 and m_2 that lead to mergers is given by

$$f_m(\sigma_1, \sigma_2) = \frac{1}{\sigma_1\sqrt{2\pi}}\int_{-\infty}^{\infty} \mathrm{e}^{-\left(\frac{v_1}{\sqrt{2}\sigma_1}\right)^2} \left[\mathrm{erf}\Big(\frac{v_1 + v_{stick}}{\sqrt{2}\sigma_2}\Big) - \mathrm{erf}\Big(\frac{v_1 - v_{stick}}{\sqrt{2}\sigma_2}\Big)\right]\mathrm{d}v_1. \tag{B2}$$

Using this definition of f_m the Smoluchowski equation becomes

$$\frac{\partial n}{\partial t} = \frac{1}{2V}\int_0^\infty n(m', t)n(m - m', t)K(m', m - m') \times f_m(\sigma_{m'}, \sigma_{m-m'})\,\mathrm{d}m' - \frac{n(m, t)}{V}\int_0^\infty n(m', t)K(m, m')f_m(\sigma_m, \sigma_{m'})\,\mathrm{d}m'. \tag{B3}$$

As discussed in Section 3.2, clouds of mass m may gain or lose kinetic energy in three ways: clouds of mass m' and $m - m'$ may merge to form extra clouds of mass m. Clouds of mass m may merge

with clouds of any other mass to decrease the number of clouds of mass m. Finally clouds of mass m can interact gravitationally with any other clouds, thus losing kinetic energy. These three processes are termed gain, loss and cooling.

Gain processes may be represented in the following way, where we have integrated over m' such that the two particles that merge have masses that sum to m:

$$\dot{E}_{\rm gain} = \int_0^\infty \int_{v_1=-\infty}^{v_1=\infty} \int_{v_2=v_1-v_{\rm stick}}^{v_2=v_1+v_{\rm stick}} [P(v_1)P(v_2)n(m',t) \; n(m-m',t)K(m',m-m')f_m(m',m-m')E_{\rm f}] \; {\rm d}v_2\,{\rm d}v_1\,{\rm d}m'. \tag{B4}$$

$P(v_1)$ and $P(v_1)$ are the probability distribution velocities v_1 and v_2 and are assumed to be Gaussian with standard deviations σ_1 and σ_2, respectively. $E_{\rm f}$ represents the final kinetic energy of a collision between particles of masses m' and $m - m'$. $E_{\rm f}$ is evaluated by considering conservation of momentum,

$$E_{\rm f} = \frac{1}{2}\frac{(m'v_1 + (m-m')v_2)^2}{m^2}. \tag{B5}$$

Equation (B4) then becomes

$$\dot{E}_{\rm gain} = \frac{n(m',t)}{2\pi}\int_0^\infty n(m-m',t)K(m',m-m') \int_{-\infty}^{\infty}\int_{v_1-v_{\rm stick}}^{v_1+v_{\rm stick}} \frac{1}{\sigma_{m'}\sigma_{m-m'}} {\rm e}^{-\left(\frac{v_1}{\sqrt{2}\sigma_{m'}}\right)^2} {\rm e}^{-\left(\frac{v_2}{\sqrt{2}\sigma_{m-m'}}\right)^2} \frac{1}{2}\left\{\frac{[m'v_1+(m-m')v_2]^2}{m}\right\} {\rm d}v_2\,{\rm d}v_1\,{\rm d}m', \tag{B6}$$

and equation (B6) may be written in the form

$$\dot{E}_{\rm gain} = \frac{n(m',t)}{2\pi}\int_0^\infty n(m-m',t)K(m',m-m') \int_{-\infty}^{\infty} \frac{1}{\sigma_{m'}\sigma_{m-m'}} {\rm e}^{-\left(\frac{v_1}{\sqrt{2}\sigma_{m'}}\right)^2} \int_{v_1-v_{\rm stick}}^{v_1+v_{\rm stick}} {\rm e}^{-\left(\frac{v_2}{\sqrt{2}\sigma_{m-m'}}\right)^2} \frac{1}{2}\left\{\frac{[m'v_1+(m-m')v_2]^2}{m}\right\} {\rm d}v_2\,{\rm d}v_1\,{\rm d}m'. \tag{B7}$$

The total kinetic energy of particles of mass m may also be decreased by mergers between particles of mass m and any other mass (the second process in the list). Similarly to equation (B6), the rate of energy loss may be written in the form

$$\dot{E}_{\rm loss} = \frac{n(m,t)}{2\pi} \int_0^\infty n(m',t)K(m,m') \int_{-\infty}^{\infty} \frac{1}{\sigma_m\sigma_{m'}} {\rm e}^{-\left(\frac{v_1}{\sqrt{2}\sigma_m}\right)^2} \int_{v_1-v_{\rm stick}}^{v_1+v_{\rm stick}} {\rm e}^{-\left(\frac{v_2}{\sqrt{2}\sigma_{m'}}\right)^2} \frac{m v_1^2}{2}\,{\rm d}v_2\,{\rm d}v_1\,{\rm d}m'. \tag{B8}$$

Finally, the total energy of particles with mass m may be decreased by collisions between particles of mass m and particles of any other mass that occur at relative velocities greater than $v_{\rm stick}$. In this case, the velocity of both particles is decreased by a factor η relative to the centre of mass. For a collision between particles of masses m_1 and m_2 (velocities v_1 and v_2), the final velocity of particle 1 (denoted v_1') is evaluated by conservation of momentum:

$$\begin{aligned} v_1' &= \eta(v_1 - v_{\rm com}) + v_{\rm com}, \\ v_{\rm com} &= \frac{m_1v_1 + m_2v_2}{m_1+m_2}, \\ \Delta E7 &= \frac{1}{2}m_1v_1'^2 - \frac{1}{2}m_1v_1^2. \end{aligned} \tag{B9}$$

Using these definitions, the change in energy of a particle of mass m_1 by gravitational cooling with a particle of mass m_2, denoted by ϵ is given by

$$\epsilon = \frac{m_1}{2}\left[v_1^2(1-\alpha^2) - v_2^2\beta^2 - v_1v_2\alpha\beta\right], \tag{B10}$$

where

$$\alpha = \eta + \frac{m_1}{m_1+m_2}(1-\eta) \tag{B11}$$

$$\beta = \frac{m_2}{m_1+m_2}(1-\eta). \tag{B12}$$

In a similar way to equation (B6) the energy loss via this process may be written in the form

$$\dot{E}_{\rm cool} = \frac{n(m,t)}{2\pi}\int_0^\infty n(m',t)K(m,m') \int_{-\infty}^{\infty} \frac{1}{\sigma_m\sigma_{m'}} {\rm e}^{-\left(\frac{v_1}{\sqrt{2}\sigma_m}\right)^2} \int^{|v_1-v_2|>v_{\rm stick}} \epsilon {\rm e}^{-\left(\frac{v_2}{\sqrt{2}\sigma_{m'}}\right)^2} {\rm d}v_2\,{\rm d}v_1\,{\rm d}m'. \tag{B13}$$

APPENDIX C: THE SOLUTION OF THE COAGULATION EQUATIONS

In our simulations we solve the discrete versions of equations (B3), (5) and (6), where by assuming that cloud mass is quantized into N bins characterized by an index, i, where $M_i = iM_0$ we can write

$$\dot{n}_k = \frac{1}{2V}\sum_{i+j=k} K_{ij}f_{ij}^{\rm m}n_in_j - \frac{n_k}{V}\sum_{j=1}^{j_{\rm max}} K_{jk}f_{ij}^{m}n_j, \tag{C1}$$

$$\dot{E}_k = \dot{E}_{\rm gain} - \dot{E}_{\rm loss} - \dot{E}_{\rm cool}, \tag{C2}$$

$$\dot{\sigma}_k = \frac{\dot{E}_k - \frac{1}{2}\sigma_k^2M_k\dot{n}_k}{\sigma_kn_kM_k}, \tag{C3}$$

where subscripts represent different mass bins. $K_{ij} \equiv K(M_i, M_j) \equiv K(iM_0, kM_0)$. The superscript 'm' represents that f is a cross-section for particle mergers.

To demonstrate the technique for solving these equations, we will consider the numerical solution of the simple Smoluchowski (equation B1), which when written in a discrete form takes on the following form:

$$\dot{n}_i = \frac{1}{2V}\sum_{j=1}^{i-1} n_jn_{i-j}K_{ij} - \frac{n_i}{V}\sum_{j=1}^{N} n_jK_{ij}. \tag{C4}$$

© 2007 The Authors. Journal compilation © 2007 RAS, MNRAS **376,** 1588–1610

Following Benson, Kamionkowski & Hassani (2005) equation (C4) can be rewritten in the form of a matrix equation

$$\dot{\boldsymbol{n}} = \mathbf{B} \cdot \boldsymbol{k}, \tag{C5}$$

where the vector $\boldsymbol{k}$ has $N \times N$ elements corresponding to $K(m_i, m_j)$. The kernel matrix, $\mathbf{B}$ has $N \times N \times N$ elements and may be written more explicitly as

$$\dot{n}_i = \sum_{jk} B_{ijk} k_{jk}, \tag{C6}$$

where

$$B_{ijk} = \frac{n_j n_k}{V}\left(\frac{1}{2}\delta_{i,j+k} - \delta_{ik}\right), \tag{C7}$$

δ represents a Kronecker delta function. We solve equation (C5) implicitly using an iterative method.

The solution of the equations that govern energy exchange between clouds (equations B7, B8 and B13) is the same as for the solution of the Smoluchowski equation in that we will write the equations in the form of the linear multiplication of two matrices and then solve this equation implicitly. In order to simplify the notation in this section, we will denote the terms in the three equations that are inside the integrals over velocity as ξ. Explicitly for the case of the equation for energy gain (equation B7):

$$\xi^{\mathrm{G}}(m, m') = \frac{1}{2\pi}\int_{-\infty}^{\infty} \frac{1}{\sigma_m \sigma_{m'}} \mathrm{e}^{-\left(\frac{v_1}{\sqrt{2}\sigma_m}\right)^2} \times \int_{v_1 - v_{\mathrm{stick}}}^{v_1 + v_{\mathrm{stick}}} \frac{1}{2} \mathrm{e}^{-\left(\frac{v_2}{\sqrt{2}\sigma_{m'}}\right)^2} \left[\frac{(m v_1 + m' v_2)^2}{m}\right] \mathrm{d}v_2 \, \mathrm{d}v_1. \tag{C8}$$

The corresponding terms in the equations for energy loss (B8) and cooling (13) are denoted by $\xi^{\mathrm{L}}(m_1, m_2)$ and $\xi^{\mathrm{C}}(m_1, m_2)$, respectively. Note that the definitions of ξ include the factors of 2π and $\frac{1}{\sigma}$ throughout the equations.

The equation for the total evolution of the energy of a system of coagulating and cooling particles may be written in terms of these new functions as

$$\begin{aligned}\dot{E}(m) = &\int_0^{\infty} n(m', t) n(m - m', t) K(m', m - m') \\ &\times \xi^{\mathrm{G}}(m', m - m') \, \mathrm{d}m' \\ &- n(m, t) \int_0^{\infty} n(m', t) K(m, m') \xi^{\mathrm{L}}(m, m') \, \mathrm{d}m' \\ &- n(m, t) \int_0^{\infty} n(m', t) K(m, m') \xi^{\mathrm{C}}(m, m') \, \mathrm{d}m',\end{aligned} \tag{C9}$$

which when discretized and rearranged becomes

$$\dot{E}_i = \sum_{j=1}^{i-1} n_i n_j K_{ij} \xi_{ij}^{G} - n_i \left[\sum_{j=1}^{N} n_j K_{ij} \left(\xi_{ij}^{\mathrm{C}} + \xi_{ij}^{\mathrm{L}}\right)\right]. \tag{C10}$$

The subscripts represent different mass bins $[n_j \equiv n(jM_0)]$. Our goal is to rewrite equation (C8) in the form of a linear multiplication of two matrices:

$$\dot{\boldsymbol{E}} = \mathbf{C} \cdot \boldsymbol{k}, \tag{C11}$$

where $\boldsymbol{k}$ is defined in the same way in the solution of the Smoluchowski equation, that is, $k_{ij} \equiv K(m_i, m_j)$. The form of C_{ijk} that is consistent with equation (C8) is given by

$$C_{ijk} = n_j n_k \left[\delta_{i,j+k} \xi_{jk}^{\mathrm{G}} - \delta_{ik}\left(\xi_{jk}^{\mathrm{C}} + \xi_{jk}^{\mathrm{L}}\right)\right]. \tag{C12}$$

This form for C_{ijk} is functionally equivalent to B_{ijk} (equation (C7)) so the solution may proceed in exactly the same way as for the Smoluchowski equation, the only difference is the form of the matrix $\boldsymbol{B}$.

The calculation of the quantities ξ^{G}, ξ^{C} and ξ^{L} is computationally very expensive so they are initialized once into a look-up table at the start of every simulation and obtained by bilinear interpolation thereafter.

This paper has been typeset from a TEX/LATEX file prepared by the author.